J. Fluid Mech. (1990), *vol.* 212, *pp.* 557–592
Printed in Great Britain

Turbulent fountains in an open chamber

By W. D. BAINES,[1] J. S. TURNER[2] AND I. H. CAMPBELL[2]

[1] Department of Mechanical Engineering, University of Toronto, Ontario, M5S 1A4, Canada

[2] Research School of Earth Sciences, The Australian National University, GPO Box 4, Canberra, ACT 2601, Australia

(Received 29 March 1989)

The flow and density distribution produced by injecting dense fluid upwards at the bottom of a homogeneous fluid have been investigated experimentally and theoretically. Both axisymmetric and line sources have been studied using small-scale laboratory experiments in which salt water is injected into a tank of fresh water. The turbulent fountain formed in this way rises to a maximum height which can be related to the Froude number of the inflow, and then falls back and spreads out along the floor. Continuing the inflow builds up a stable stratification in a similar manner to that discussed earlier for the 'plume filling box model' of Baines & Turner (1969) which is complementary to the present work. The fountain flows considered here have the important new feature that the volume of the inflow is significant, so the total volume of fluid in the 'open' container increases with time. The evolution is determined by the rate of entrainment into the fountain from its surroundings, which is found directly by experiment. Re-entrainment of fluid into the fountain continually changes the density profile in the mixed fluid collecting at the bottom of the chamber below the level of the fountain top, and controls the rate of rise of a 'front' of marked fluid. The top of the fountain rises linearly in time, at a rate which, for axisymmetric fountains, has been shown both experimentally and theoretically to be close to half the rate of rise of the free surface due to the inflow. Thus at a certain time the front rises above the top of the fountain. Once the mixed fluid at the bottom of the chamber has risen above the fountain its density profile remains unchanged. The front velocity, the fountain height and the density profile have all been obtained as functions of time using a theory which is in good agreement with the experimental results for a large range of input Froude numbers. For line fountains the results are less precise owing to an instability which causes the flow to switch irregularly from a symmetrical state to one in which the downflow occurs on one side only, and with a smaller maximum height. In concluding we discuss the applications which motivated the work, particularly the development of a stratified hybrid layer in magma chambers replenished from below, and the dynamically identical, but inverted problem of heating large buildings through ducts located near the roof.

1. Introduction

The problem of convection from a small source in a confined region was first solved explicitly twenty years ago (Baines & Turner 1969). In that paper we calculated the effect of continuous convection from point or line sources of buoyancy alone on the properties of the surrounding fluid, which was originally uniform in density and of fixed volume. In particular it was shown that an asymptotic state is attained, in

which the density profile is fixed in shape, but the density is increasing (or decreasing) at a constant rate at all levels, as a result of the combined effects of entrainment into the plume and vertical advection in the environment. This kind of problem is now generally referred to as 'the filling box model', but perhaps it should more correctly be called the 'plume filling box model' because it considered only the case where buoyancy and the resulting momentum act in the same direction.

In carrying out experiments to test the theoretical results it was convenient to use sources of concentrated salt solution flowing downwards into a tank of fresh water to form a turbulent plume. The momentum of the inflow was kept as small as possible so that it approximated to a pure buoyancy source, but inevitably a small extra volume flux was added, which could be ignored for the purpose of evaluating the theory. Modifications have subsequently been made to take account of the momentum flux (Baines & Murphy 1986) and of the changing volume of the region under consideration, due either to the input or to the entrainment of fluid across an interface bounding the layer (Baines 1975; Kumagai 1984). In each of these cases the addition of extra fluid makes only a small difference to the calculations.

The flows studied in this paper are related to the above filling box problems, but they arise in practical situations where the input of a large volume of source fluid cannot be ignored. Another essential difference is that the initial momentum and buoyancy act in opposite directions so that, for example, dense fluid ejected upwards is acted on by buoyancy forces which reverse its motion, and finally falls back around the upflow in the form of a 'fountain'. The 'fountain filling box model' is therefore the complementary problem to the plume filling box. Both have wide applications in engineering and in nature. For example, when a room is heated in winter by forcing hot air through vents in the floor, the plume filling box model is appropriate. In summer, when the room is being cooled by forcing cold air through the same vents, it is the fountain filling box model that must be used. The various applications will be discussed in more detail in a later section, but two of them which provided the original motivation for the work reported here will be mentioned now. Campbell & Turner (1989) have applied the results of preliminary experiments of this kind to magma chambers, replenished from below with a turbulent input of hot magma which is denser than that already in the chamber. They have shown that this new magma can be injected with enough upward momentum to rise high into the chamber and mix extensively with the resident magma and fall back to form a hybrid layer. One of us (W. D. B.) has been concerned with the ventilation of large open structures such as aircraft hangars, which are heated using ceiling-mounted fans to drive hot air towards the floor. The flow produced in this case is the inverted equivalent of the replenished magma chamber, and both of these can be studied and the evolution of the density structure understood using laboratory models in which dense salt solution is injected upwards into fresh water.

The meaning of the term 'open chamber' in the present context should be made clear. In the laboratory analogue experiments it means that the surface of the fluid is free to rise at the rate of injection of the dense fluid, and that the front of the mixed fluid and the density structure below it are evolving in an environment which is moving upwards at this mean rate. In the applications it implies that any removal of fluid from the region of interest must take place above the level of the front, from the region that is not affected by the mixing. For example, in a magma chamber the injection of dense magma at the bottom can be compensated for by expansion of the chamber or by the eruption of an equal volume of the original magma at the top. In a ventilated building cold air might be allowed to flow out near the floor at the same

rate as heated air is injected at the top. It is quite different from the case where both inflow and outflow are behind the front, corresponding for instance to an intake into the ventilation system being located near the ceiling. The evolution of this latter case is the subject of a separate study (Baines & Reedman 1990), and for our present purposes we need to note only that it leads to the formation of a sharp interface between the injected and the original fluid, located at the height of the top of the fountain, quite different from the behaviour described in this paper.

In addition to the work already referred to there are several papers that provide relevant background to the present study. Morton (1959) produced a theory for forced plumes which indicates that, in the case where the momentum and buoyancy are opposing, the flow is little affected by buoyancy till very close to the level where it is brought to rest, and also predicts the way in which the penetration depth depends on the external parameters. Though this theory ignored the effect of the opposing return flow (the outside of the fountain), experiments by Turner (1966) using salt fountains injected upwards into fresh water verified Morton's functional dependence of the height on the momentum and buoyancy fluxes, and obtained numerical values for the steady fountain height which will be used in the present study. Turner (1966) did not address the problem of a changing environment – all the fluid falling back from the fountain was removed below the level of the source and did not build up as a layer which was re-entrained into the fountain. Seban, Behnia & Abreau (1978) studied heated air jets discharged downwards, and concluded that the penetration depth and the centreline temperatures could be adequately predicted using a theory based on the downward flow alone, though their radial temperature profiles gave evidence of a substantial interaction between the two parts of the flow. The most thorough experimental study of a two-dimensional fountain is that of Goldman & Jaluria (1986). They used hot air blown downwards from a slit into a chamber of air at room temperature to simulate motions generated by fires in an enclosure. They measured the penetration distance and the velocity and temperature profiles for both free and wall jets, and showed that the major parameter determining the flow is a Froude number, as will be discussed in detail in following sections. They concluded that the effect of the opposing buoyancy is very important in many problems of practical interest. Note, however, that in this experiment too the environment was not evolving in time, and a steady state was attained by allowing the heated air to flow out of the enclosure at its open top. The experiments and related theory presented below are designed to remove this limitation, and to study explicitly the evolution of the coupled flows in the fountain and its surroundings.

2. Description of the flow

Before presenting the detailed experimental results and the associated theory, we shall describe the laboratory experiments in qualitative terms and the physical ideas needed to interpret them. The basis for the quantitative model developed will then become clearer. The first experiments on turbulent fountains are described in Turner (1966) and a discussion of the experiments that led up to the present fully quantitative study is to be found in Campbell & Turner (1989).

The experiment consists simply of ejecting a turbulent jet of salt solution upwards from a nozzle projecting some distance above the bottom of a tank containing fresh water. The general arrangement and the notation used in the rest of the paper are sketched in figure 1. (The case of a vertical round outlet will be described first, though other configurations have also been studied.) The jet rises into the environment and

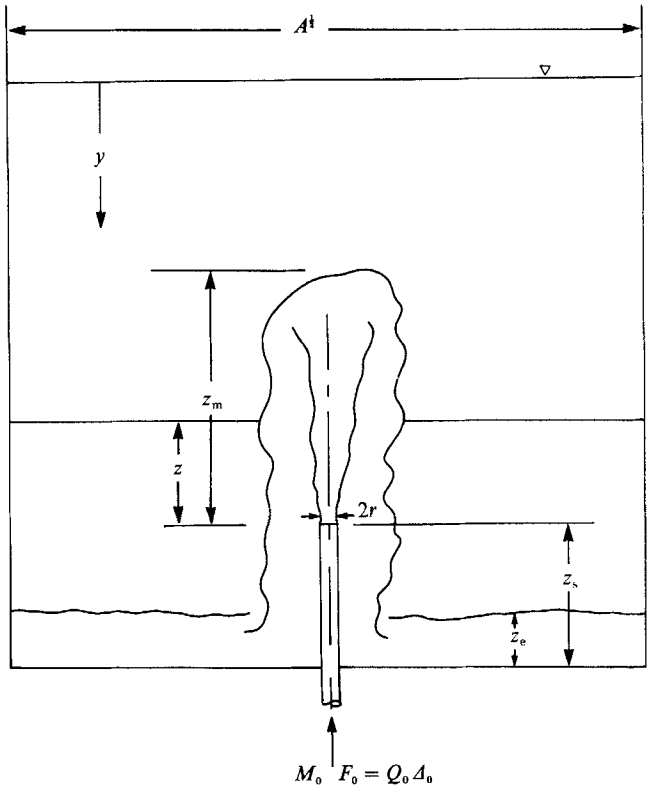

FIGURE 1. Definition sketch for the flow in a circular fountain.

loses momentum steadily due to the opposing buoyancy forces. The injected fluid reaches a maximum height and falls back around the upflow, accelerating as it does so. The upflow is now mixing with downward-moving fluid which is also denser than the environment, so that the height of the top of the fountain falls from its initial height to a steady mean value z_m, about which there are small random fluctuations. With a source inclined at a small angle to the vertical z_m does not decrease, since the upflow and downflow regions are then separated and do not interfere with one another. When the downflow reaches the bottom of the tank it spreads out sideways to form a denser layer of fluid. During the experiment, in particular when the jet flow is first turned on, a neutrally buoyant dye marker is injected to mark a volume of fluid which has been in the fountain at a particular time.

The first heavy fluid to reach the bottom has a small density discontinuity above it (the first front). The turbulence in this layer quickly dies out, and provided the

FIGURE 2. Photographs of fronts produced by axisymmetric fountains. (*a*) and (*b*) relate to experiment A9 in which the source was vertical; $r_0 = 0.091$ cm, $Q_0 = 4.83$ cm^3 s^{-1}, $A_0 = 43.1$ cm s^{-2}, $Fr_i = 93.8$. (*a*) The early stage $t = 2$ min 30 s after the start of the flow showing the fountain rising high above the first front. The flow is marked by a suspension of mica flakes. (*b*) Much later ($t = 2$ h 0 min after the start). The front, marked by fluorescein dye, has risen above the top of the fountain, which was made visible by the injection of fresh dye through the inclined tube shortly before the photograph was taken. (*c*) An inclined fountain and the associated front (experiment A8, with $r_0 = 0.187$ cm, $Q_0 = 13.8$ cm^3 s^{-1}, $A_0 = 84.4$ cm s^{-2}, $Fr_i = 31.9$ at $t = 6$ min 30 s), showing the separation of the up- and downflows.

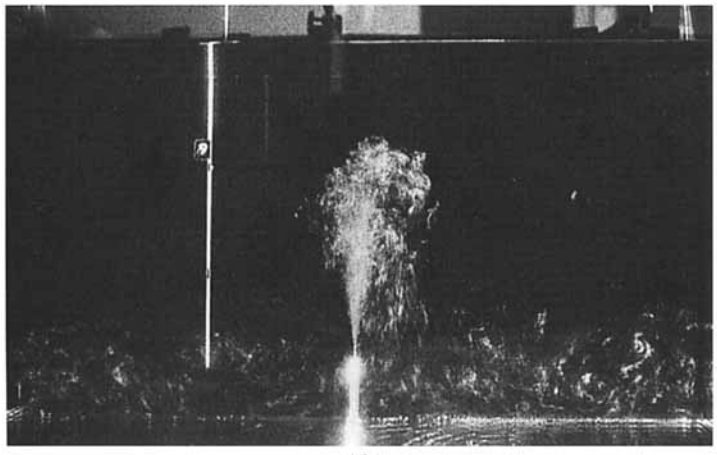

(*a*)

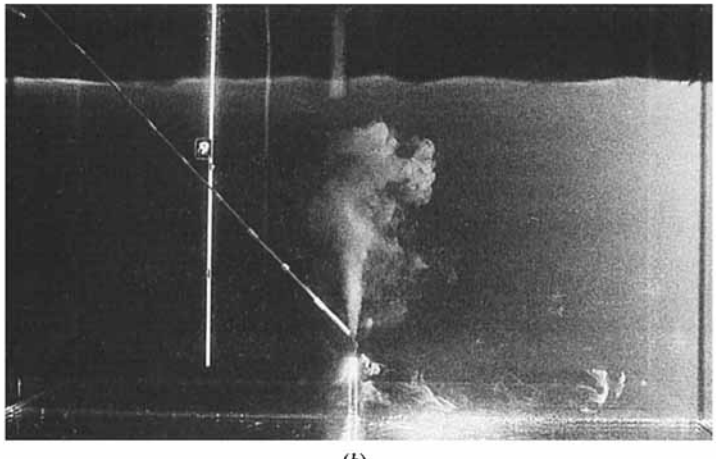

(*b*)

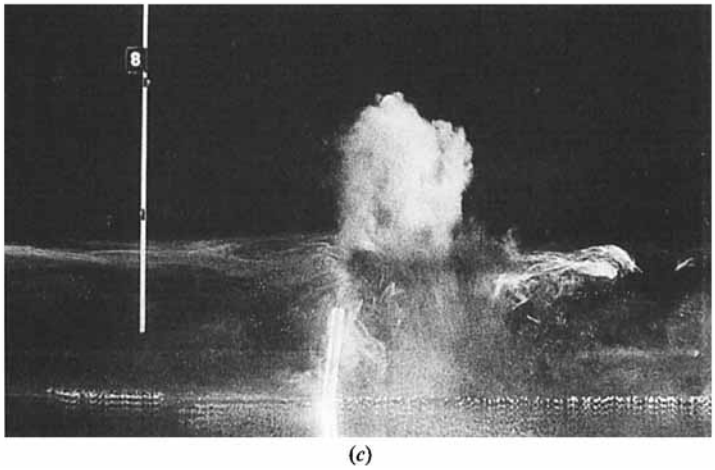

(*c*)

FIGURE 2. For caption see facing page.

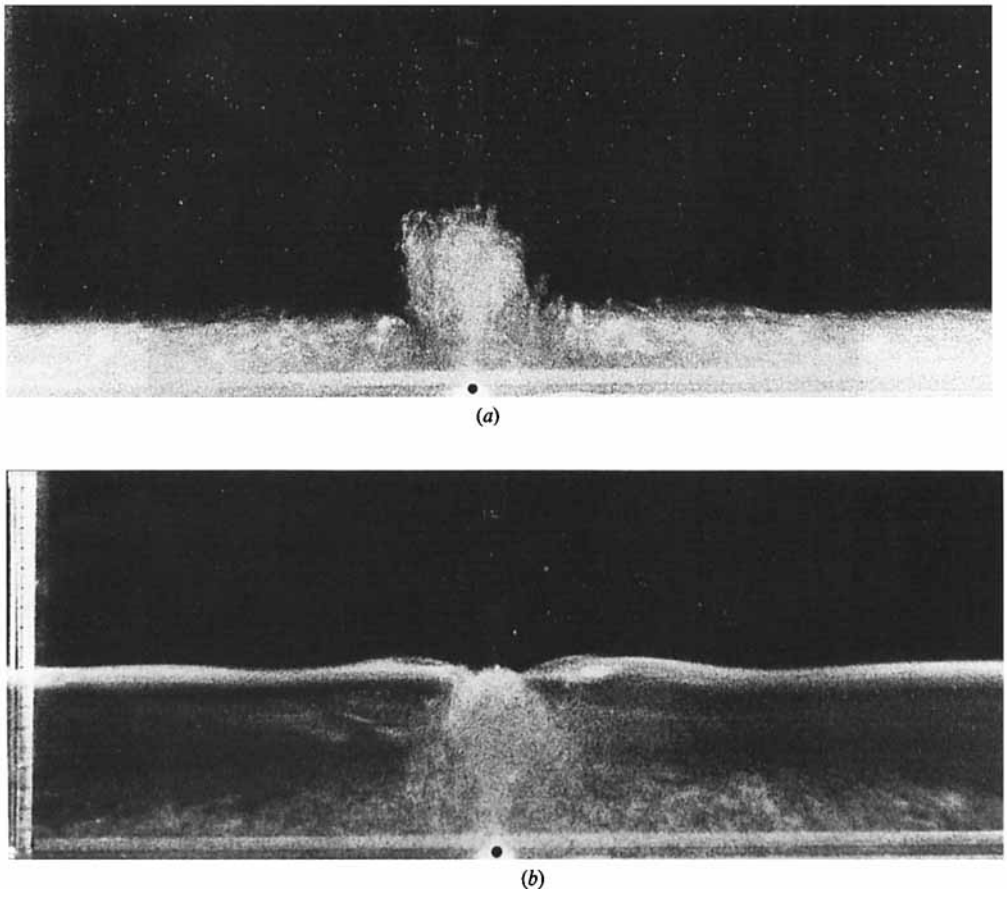

(a)

(b)

FIGURE 3. The front produced by a symmetrical line fountain (experiment B7, with $b_0 = 0.00164$ cm, $q_0 = 0.464$ cm^2 s^{-1}, $A_0 = 73.2$ cm s^{-2}). (a) $t = 30$ s: the top of the fountain is above the first front; (b) $t = 4$ min: the first front has just passed the top of the fountain, and is being deflected downwards by the entrainment.

tank is sufficiently wide compared with the fountain height, the fluid in this layer can be regarded as part of the environment so far as the continuing flow in the fountain is concerned. Because the bottom layer is denser than the original fresh water, the outer part of the fountain that entrains it arrives at the bottom of the tank even heavier and flows underneath. The first front is pushed upwards, and a stable density gradient develops in the hybrid layer below it, just as it would if a dense plume were injected at the level of the top of the fountain (Baines & Turner 1969). If more dye is added to the jet at a later time it too spreads along the bottom and is lifted as a horizontal layer. During the early stages of an experiment the fountain entrains mainly the fluid above the front and so the front rises rapidly, with the 'mixed' layer consisting of a small fraction of the input fluid and a larger volume of the environment which has been mixed into it; this is the stage pictured in figure 2(a).

As filling continues and the hybrid layer grows, the fountain entrains less of the environment fluid above the front, and more of the gradient region below the front is recycled into the fountain. Thus the mean density of the hybrid layer continually

increases, and since the height of rise of the fountain is determined by the difference in density between the fountain and its immediate surroundings, a fixed input momentum flux raises the fountain to steadily increasing elevations. The rate of rise of the first front is reduced as the net entrainment of environmental fluid decreases, but it remains greater than the rate of rise of the top of the fountain. At a certain height and time (which we shall determine) it overtakes the fountain and rises above, it, as shown in figure 2(*b*). After this time the fluid above the first front can no longer be entrained into the fountain, and so the rate of advance of the front is controlled entirely by the rate at which fluid is added to the tank. The density structure above the top of the fountain cannot be further affected by the fountain and is advected upwards with the density it had when it passed the fountain top. The density profile below the top of the fountain at any time continues to be modified by the combination of advection and re-entrainment. It was the recognition of these two distinct stages, and the need for a careful treatment of the second which has no equivalent in the 'plume filling box' problem, which has led to the work reported here.

Line fountains evolve in a similar way, as shown in the two photographs of figure 3, taken when the first front was respectively below and above the top of the fountain. A new feature was observed in this case, however, which was quite different from the behaviour of the axisymmetric fountain. A symmetrical downflow each side of the upflowing jet could not be maintained indefinitely; at intervals the fountain became unstable and all the downflow moved off to one side for a time. There was a marked decrease in the height of the fountain during this period, while the height of the front on that side increased more rapidly as more fluid was supplied to it. This behaviour will be discussed in more detail in §4.2 (see also figure 11).

In the following section we present the work on axisymmetric fountains. After describing the experimental methods, we discuss several illustrative plots of the data as a further aid to understanding the principles involved. The detailed theory for the motion of fronts and the evolution of the density profiles is then developed and compared with the measurements. The corresponding results for line fountains are presented in §4. In the final section we discuss and sum up the results and comment on their application to the problems that motivated the study and to a wider range of related flows.

3. Axisymmetric sources

3.1. *Experimental methods*

All of the experiments were conducted in a tank made of acrylic plastic 60 cm deep and 70 cm square in horizontal cross-section. It was partially filled with tap water and then salt water was introduced through a source in the centre of the base, using a pump and flow meter in the supply line to control and monitor the flow rate. The source fluid issued from a straight length of tubing of either 6, 4, 2 or 1 mm inside diameter and each tube was 10 diameters in length to give a uniform flow at the outlet. In every experiment the flow in the source tubing was laminar but the jet issuing into the fresh water was turbulent within 3 mm of the outlet. Experiments were conducted both with the outlet vertical, or at a small angle to the vertical (arbitrarily set at 7°; see figure 2*c*).

The controlling parameter in the rise of the fountain is the Froude number, the determination of which requires the volume, momentum and buoyancy fluxes to be

specified. The first and third are easily metered at the source but the momentum flux depends on the velocity distribution at the outlet. One might assume from the start that the flow in the outlet pipe is laminar, but this was checked directly by testing each source as a weakly buoyant jet as follows. Fresh water containing a marker dye was injected into the tank which contained salt water. A front formed at the free surface when the jet impinged on it and this front could be followed and its elevation measured as it progressed down toward the source elevation. This is the method used by Baines & Turner (1969) to evaluate the entrainment coefficient. In the case of jet-like flow a plot of the logarithm of elevation above the virtual source against time yields a straight line. (Thus the actual position of the virtual source may be determined by varying the assumed location of the source until a straight line is obtained. It was found that the source was in fact at the end of the outlet pipe, and this was verified by tracing the outline of the jet back to the source.) The slope of the line is proportional to the entrainment coefficient and the square root of the momentum flux. Taking the entrainment coefficient to be 0.057, the momentum flux for each source corresponded to that of a flow with constant velocity across a hole having a diameter of 0.83 times the tube diameter. This value is close to $\sqrt{3}/2 = 0.866$, the value to be expected for laminar flow in the tube.

During each experiment measurements were made of the height of the fountain, the elevation of fronts in the environment and the density distribution within the environment. The fountain and fronts were made visible by injecting 5 cm^3 of either a suspension of mica flakes or fluorescein dye into the source line. Usually the flakes were used at the start of the test and produced a white first front. Fluorescein was introduced later to mark other levels in the flow, which we have called the second and third fronts. Precise illumination was provided by photographic floodlights shone through 1 cm wide vertical slits in the sides of the tank. The back of the tank was covered with black paper and the room was darkened to produce sharp photos. Elevations were recorded by photography for the first few minutes as the fronts moved rapidly and later, as the fronts sharpened, the level could be read to an accuracy of 1 mm by eye.

Measurements of fountain height were also made both from photographs and visually. During the hour or two duration of a typical experiment photographs were taken at regular intervals and the fountain height as well as the location of fronts was recorded. This can be seen in the steady progression of the fronts in figure 4. However, the scatter of the fountain height measurements is much larger than the accuracy of individual measurements as can also be seen in figure 4. The top of the fountain oscillated over several centimetres with periods of the order of minutes. A separate set of experiments was conducted in which the fountain was observed for several minutes and a single representative mean value was recorded. The scatter in data obtained in this way was much less.

It was found that starting or stopping the source did not disturb the fronts, so density profiles could be taken at any time by stopping the flow to the source. A syringe was connected to length of tubing 0.5 mm in diameter and the end placed at a measured elevation. About 5 cm^3 of water was removed and the density determined using an Anton Paar density meter. The accuracy of determination was about 10^{-5} g cm^{-3} but the plot of results from a typical experiment in figure 5 shows that the scatter is about 10 times larger. This is due to the inaccuracy in holding the elevation of the sampling tube constant during removal of a sample and the uneven withdrawal rate. The data in figure 5 have been plotted relative to the free surface

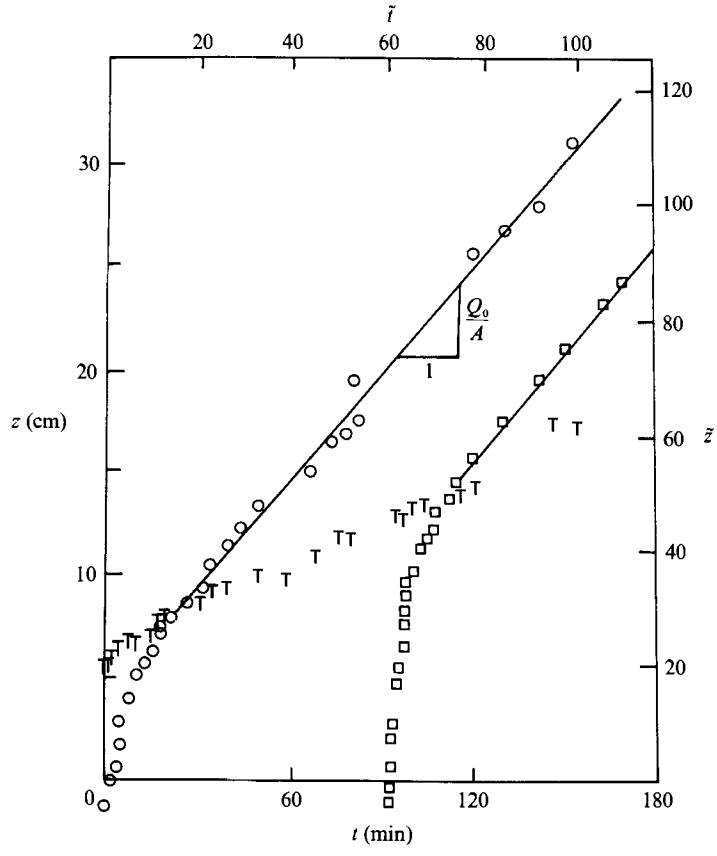

FIGURE 4. The measured elevations of two fronts and the top of the fountain as functions of time for experiment A17 ($r_0 = 0.271$ cm, $Q_0 = 14.6$ cm^3 s^{-1}, $A_0 = 162.8$ cm s^{-2}, $Fr_i = 8.94$). ○, first front; □, second front; T, height of fountain. The lines drawn correspond to the rate of rise of the free surface.

to show, as we have discussed above, that after the first front reaches the top of the fountain the density profile has an unchanging form in the region above the top. Below the top the density continuously increases to approach the density of the source fluid at large times.

3.2. *Dimensionless equations and the initial fountain height*

Consider a source of heavy fluid injected with upward momentum into the bottom of an environment of lighter fluid which is infinite in extent horizontally. If the source is small compared with the height of the resulting fountain the flow will depend only on the fluxes of buoyancy F_0 and momentum M_0 defined by $M_0 = \pi r_0^2 U_0^2$ and $F_0 = \pi A_0 r_0^2 U_0$, where r_0 is the source radius, U_0 is the mean velocity at the source, and $A_0 = g(\rho_0 - \rho_i)/\rho_i, \rho_0$ being the density of the input fluid and ρ_i the initial density of the environment. It will not depend explicitly on the volume flux $Q_0 = \pi r_0^2 U_0$, once the position of the virtual source has been determined. As shown in Turner (1966) the height of the fountain is defined by dimensional consistency as

$$z_m = \text{constant} \times M_0^{\frac{3}{4}} F_0^{-\frac{1}{2}}. \tag{1}$$

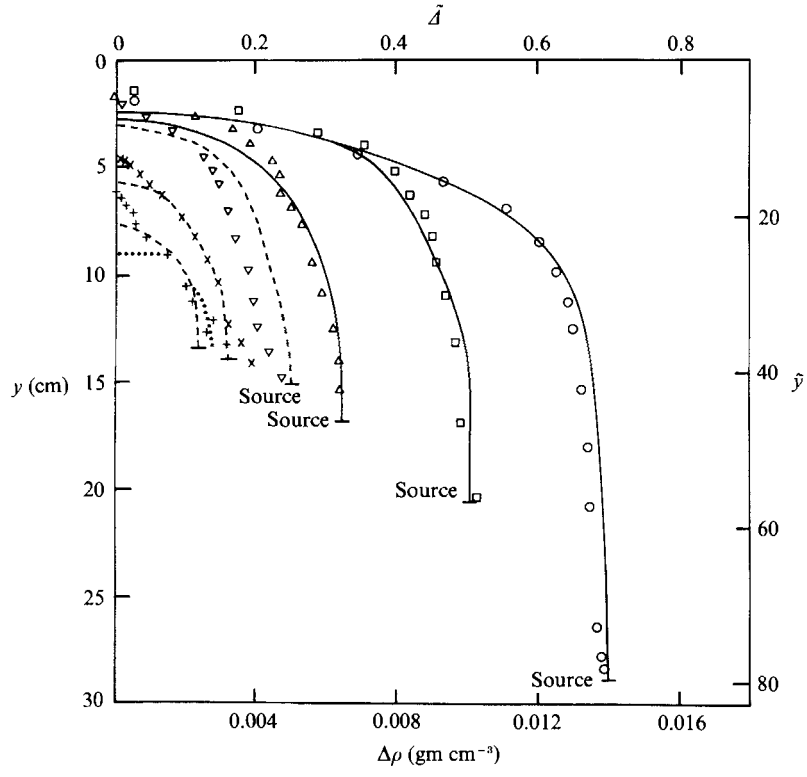

FIGURE 5. Density profiles plotted as a function of the depth below the free surface for the stratified layer produced by an axisymmetric fountain. The left and lower scales refer to dimensional variables, and the right and upper scales to dimensionless variables. The experiment is one carried out by Campbell & Turner (1989) but not analysed in detail in that paper. $Q_0 = 14.4$ cm^3/s, $r_0 = 0.363$ cm, $\Delta\rho_0 = 0.0201$ gm/cm^3, $Fr = 13.8$; +, $\tilde{t} = 1.6$; ×, 3.2; ▽, 6.73; △, 11; □, 22; ○, 44. The curves drawn are theoretical predictions, as discussed later in §3.4.

By the same reasoning, the total volume flux entrained by the fountain between the elevations z_m and z can be expressed as

$$Q_e = \frac{M_0^{\frac{5}{4}}}{F_0^{\frac{1}{2}}} fn\left(\frac{zF_0^{\frac{1}{2}}}{M_0^{\frac{3}{4}}}\right). \tag{2}$$

These equations can be written in a more convenient form for interpreting the experimental measurements by using the buoyancy and velocity at the source and the source radius r_0. This leads to the relations:

$$\frac{z_m}{r_0 Fr} = \text{constant}, \tag{3}$$

$$\frac{Q_e}{Q_0 Fr} = fn\left(\frac{z}{r_0 Fr}\right), \tag{4}$$

where Fr is a Froude number defined by

$$Fr = \frac{U_0}{(r_0 \Delta_0)^{\frac{1}{2}}} = \frac{Q_0}{\pi r_0^{\frac{5}{2}} \Delta_0^{\frac{1}{2}}}. \tag{5}$$

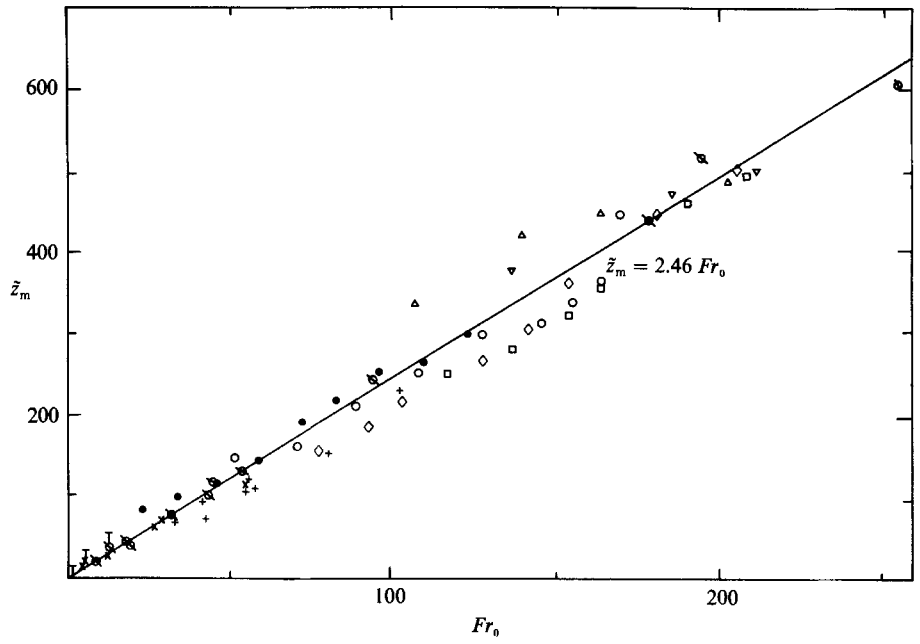

FIGURE 6. Dimensionless height of a circular fountain with a vertical source, as a function of Froude number, measured by various observes: T, Turner (1966); ×, Seban *et al.* (1978); +, Reedman (1986 unpublished) ($r_0 = 0.073$ cm); Morala (1985 unpublished), using $r_0 = 0.073$ cm and various $\Delta\rho_0/\rho_0$: ●, 0.178; ○, 0.10; ◇, 0.06; □, 0.03; △, 0.01; ▽, 0.006; ∅, the present study (with $r_0 = 0.043$–0.187 cm).

The results of the present experiments, the values of z_m for vertical fountains, have been plotted in figure 6 in terms of the Froude number, together with the measurements made by Turner (1966) and Seban *et al.* (1978), and in unpublished experiments carried out in W.D.B.'s laboratory by T. J. Reedman (1986) and E. Morala (1985). The value 2.46 for the constant in (3) was fitted by Turner (1966) for experiments conducted at small Fr and it holds accurately over the larger range in Fr covered in figure 6. It is evident to the eye that z_m increases as the fountain is deflected from the vertical, and the measurements plotted on figure 7 for a 7° inclination follow a steeper slope as expected. The constant 2.88 shows that the height increase is about 17%. The mean height is larger, and the oscillations of the top of inclined fountains are smaller, because the turbulent downflow does not interfere with the upflow as it does for vertical fountains.

Some measurements of the entrained flux Q_e into a vertical fountain were made by T. J. Reedman (1986, personal communication), using a method developed for plumes by Baines (1983). These measurements showed a linear increase of flux with depth below z_m, indicating that (4) should be of the form

$$\frac{Q_e}{Q_0 Fr} = C - B\left(\frac{z}{r_0 Fr}\right). \tag{6}$$

The density of the environment was not monitored carefully enough in these experiments to specify the constants C and B with certainty, although since $Q_e = 0$ when $z = z_m$ we know that $C/B = 2.46$.

This simple result suggests that we might seek a more fundamental explanation of

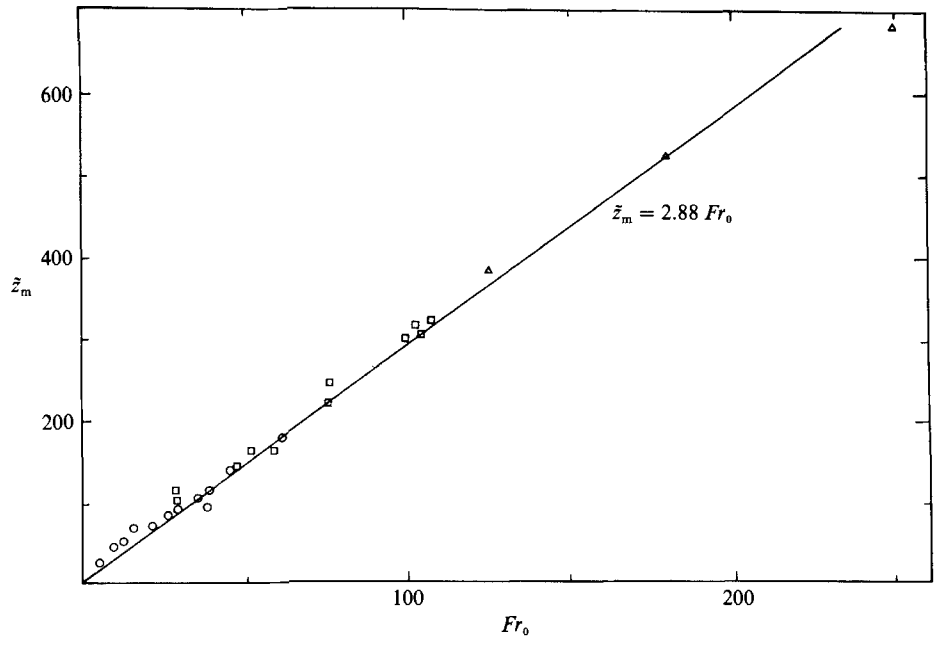

FIGURE 7. Dimensionless height of a circular fountain from a source inclined at 7° from the vertical, as a function of Froude number: △, $r_0 = 0.046$ cm; □, 0.091 cm; ○, 0.187 cm.

the rate of entrainment into a fountain, by relating it to the behaviour of the up- and downflows using Taylor's entrainment hypothesis, that the inflow is proportional to the local mean velocity. (See Batchelor 1954; Morton, Taylor & Turner 1956; Turner 1973 and the more recent survey by Turner 1986.) First, the rate of entrainment per unit area into a pure jet is proportional to z^{-1}, and the radius increases linearly with z, so that the total inflow per unit height is constant, as implied by (6). The solution for entrainment into the upflow of a negatively buoyant jet obtained by Morton (1959) showed a variation that differed little from this up to a point very close to the reversal level. However, this argument does not allow for the fact that, in a steady vertical fountain, the upflowing jet can interact with the environment only through the descending outer part of the fountain. This downflow can be thought of as a line plume, with constant buoyancy flux distributed round a ring, entraining fluid at its outer boundary and losing a small fraction of its flux to the upflow. The diameter of this annular source is determined by the upflow as it is brought to rest by the negative buoyancy, flows outwards and begins to descend. The mean vertical velocity for a line plume is constant with height, provided the change of buoyancy flux due to entrainment into the upflow can be neglected. Since the outer diameter of the fountain is also nearly constant (Turner 1966) the application of the simple entrainment assumption again leads to the result that the total inflow per unit height should be constant.

With both the experimental evidence and the above arguments in mind, (6) will be adopted for the analysis in this paper. The determination of B provides the measure of the average inflow per unit height

$$q_e = -\frac{dQ_e}{dz} = B\frac{Q_0}{r_0}, \tag{7}$$

and this is the only free parameter required to complete the theory developed below. Note that (7) indicates that the local entrainment is independent of the Froude number of the source.

3.3. *Theory for the motion of fronts*

What we have called a front is formed from dyed fluid entering the environment at the bottom, which may be below the elevation of the source. As the turbulent downflow impinges on the floor of the container it spreads over the floor as a turbulent gravity current. The turbulence may die out before the flow reaches the container walls but the layer of dyed fluid retains a finite thickness over the entire floor. The fluid which flows from the fountain mixes with some of the layer on the floor and so removes some of the dye marker. Most of the dyed fluid is pushed upward by the fluid which flows out from the fountain after the marked fluid and this forms a front about one centimetre thick. As it is pushed up by the fountain fluid it becomes thinner as the entrainment flow q_e incorporates some of it back into the downflow of the fountain.

The motion of the front is defined by writing the equation for conservation of volume flux in the layer between the floor and the top of the front at elevation z:

$$A\frac{\mathrm{d}z}{\mathrm{d}t} = Q_0 + Q_e, \tag{8}$$

where A is the cross-sectional area of the tank and z is defined on figure 1. Defining the dimensionless variables

$$\tilde{z} = \frac{z}{r}, \quad \tilde{Q}_e = \frac{Q_e}{Q_0}, \quad \tilde{t} = \frac{tQ_0}{Ar}$$

and introducing (6) in (8), we obtain

$$\frac{\mathrm{d}\tilde{z}}{\mathrm{d}\tilde{t}} = 1 + CFr - B\tilde{z}. \tag{9}$$

This is an equation which can be integrated directly to give $\tilde{z}$ as a function of $\tilde{t}$ provided that Fr can be expressed as a function of $\tilde{z}$ or $\tilde{t}$ and Fr_1, the initial value of Fr, which is the basic source parameter determining the flow in the fountain and in the surrounding environment. As time progresses the density in the layer of depth $\tilde{z}_m + \tilde{z}_s$ increases and so the relative buoyancy of the fountain fluid decreases and the Froude number increases. It will be assumed that Fr as it appears in (5) is defined by the mean density $\bar{\rho}$ in the new environment of the fountain, i.e. in the stratified layer of height $z_m + z_s$, and the corresponding $\bar{\Delta} = g(\bar{\rho} - \rho_i)/\rho_i$. Thus, defining Fr_i as the value when the front is at the source elevation

$$Fr = Fr_i(1 - \bar{\Delta}/\Delta_0)^{-\frac{1}{2}} \approx Fr_i(1 + \tfrac{1}{2}\bar{\Delta}/\Delta_0). \tag{10}$$

Linearization provides a good approximation at least for large Fr_i and until the front overtakes the top of the fountain, since $(\bar{\Delta}/\Delta_0) \ll 1$ under these conditions, as shown in §3.3.1.

The mean density $\bar{\rho}$ is always greater than ρ_i, which is the initial mean density in the environment, since it is produced by the inflow of fluid of density ρ_0 from the source. During the interval $(\tilde{t} - \tilde{t}_i)$ when the front is below $\tilde{z} = \tilde{z}_m$ all the excess dense fluid accumulates in the layer for which $\bar{\Delta}$ is defined. Thus

$$\bar{\Delta}(\tilde{z}_m + \tilde{z}_s) = \Delta_0(\tilde{t} - \tilde{t}_i) = \Delta_0 \tilde{t}_1 \tag{11}$$

say. Combining (10) and (11) leads to

$$Fr = Fr_{\mathrm{i}}\left(1+\frac{1}{2}\frac{\tilde{t}_1}{\tilde{z}_{\mathrm{m}}+\tilde{z}_{\mathrm{s}}}\right), \tag{12}$$

where $Fr_{\mathrm{i}} = (B/C)\,\tilde{z}_{\mathrm{mi}}$ from (3) and (6), and $\tilde{z}_{\mathrm{mi}}$ is defined as the initial dimensionless fountain height. The further approximation that $\tilde{z}_{\mathrm{m}}$ varies by only a small fraction of its initial value over the region of interest, i.e. putting $\tilde{z}_{\mathrm{m}} = \tilde{z}_{\mathrm{mi}}$ in the last term on the right-hand side of (12), gives

$$\tilde{z}_{\mathrm{m}} = \tilde{z}_{\mathrm{mi}}\left(1+\frac{\tilde{t}_1}{2(\tilde{z}_{\mathrm{mi}}+\tilde{z}_{\mathrm{s}})}\right) = \tilde{z}_{\mathrm{mi}}+\tfrac{1}{2}\tilde{z}_{\mathrm{r}}\tilde{t}_1, \tag{13}$$

where $\tilde{z}_{\mathrm{r}}$ is a measure of the effect of the elevation of the source above the floor.

Using the same approximation $\tilde{z}_{\mathrm{m}} = \tilde{z}_{\mathrm{mi}}$ in (12) and inserting the above relations in (9) gives the differential equation for the layer depth

$$\frac{\mathrm{d}\tilde{z}}{\mathrm{d}\tilde{t}_1} = 1+B\tilde{z}_{\mathrm{mi}}+\tfrac{1}{2}B\,\tilde{z}_{\mathrm{r}}\tilde{t}_1-B\tilde{z}. \tag{14}$$

Integration of (14) from $\tilde{z} = \tilde{z}_{\mathrm{e}}-\tilde{z}_{\mathrm{s}}$ at $\tilde{t}_1 = 0$ (where $\tilde{z}_{\mathrm{e}}$ is the height at which fluid enters the new environment of the fountain; see figure 1 and §3.4) to a general height $\tilde{z}$ gives

$$\tilde{z} = (\tilde{z}_{\mathrm{e}}-\tilde{z}_{\mathrm{s}})\,\mathrm{e}^{-B\tilde{t}_1}+\left(\tilde{z}_{\mathrm{mi}}+\frac{1}{B}\right)(1-\mathrm{e}^{-B\tilde{t}_1})+\tfrac{1}{2}\tilde{z}_{\mathrm{r}}\tilde{t}_1-\frac{\tilde{z}_{\mathrm{r}}}{2B}(1-\mathrm{e}^{-B\tilde{t}_1}), \tag{15}$$

where the first two terms on the right give the front position for a fountain of constant height and the other two terms result from adding the linear increase of fountain height with time given by (13).

The simultaneous solution of (13) and (15) for $\tilde{z} = \tilde{z}_{\mathrm{m}}$ gives the crossover time $\tilde{t}_1^*$ when the front is at the elevation of the top of the fountain $\tilde{z}_{\mathrm{m}}^*$

$$\tilde{t}_1^* = \frac{1}{B}\ln\left(\frac{1-\frac{1}{2}\tilde{z}_{\mathrm{r}}+B(\tilde{z}_{\mathrm{mi}}+\tilde{z}_{\mathrm{s}}-\tilde{z}_{\mathrm{e}})}{1-\frac{1}{2}\tilde{z}_{\mathrm{r}}}\right), \tag{16}$$

where $\tilde{z}_{\mathrm{r}} = \tilde{z}_{\mathrm{mi}}/(\tilde{z}_{\mathrm{mi}}+\tilde{z}_{\mathrm{s}})$ is assumed to be constant.

As a further check on the consistency of this solution we can substitute (13) for $\tilde{z}$ on the right-hand side of (14) and verify that $\mathrm{d}\tilde{z}/\mathrm{d}\tilde{t}_1 = 1$ at $\tilde{z} = \tilde{z}_{\mathrm{m}}^*$. Thus the solution matches smoothly into the solution for the front above the crossover point, where it rises at unit (dimensionless) rate, determined entirely by the rate of addition of fluid to the tank.

3.3.1. *Comparison with experiments*

It is now possible to assess the approximations in the analysis by using the above results together with the experimental values. The smallest Froude number studied was approximately equal to 9 with $\tilde{z}_{\mathrm{r}}$ about 0.5. The above equations indicate that $\tilde{t}_1^*$ is approximately 8 and the density ratio in (10) at the crossover is about 0.2. The height of the top of the fountain z_{m} increases by about 10% during the time the front rises from the source to z_{m} so $\tilde{z}_{\mathrm{r}}$ increases by 4%. This indicates that (10) and the solutions (15) should be revised for accurate representation at the smallest Fr. For $Fr \geqslant 20$ the approximations are much more accurate.

Equation (15) has been fitted to the measured front elevations for all of the

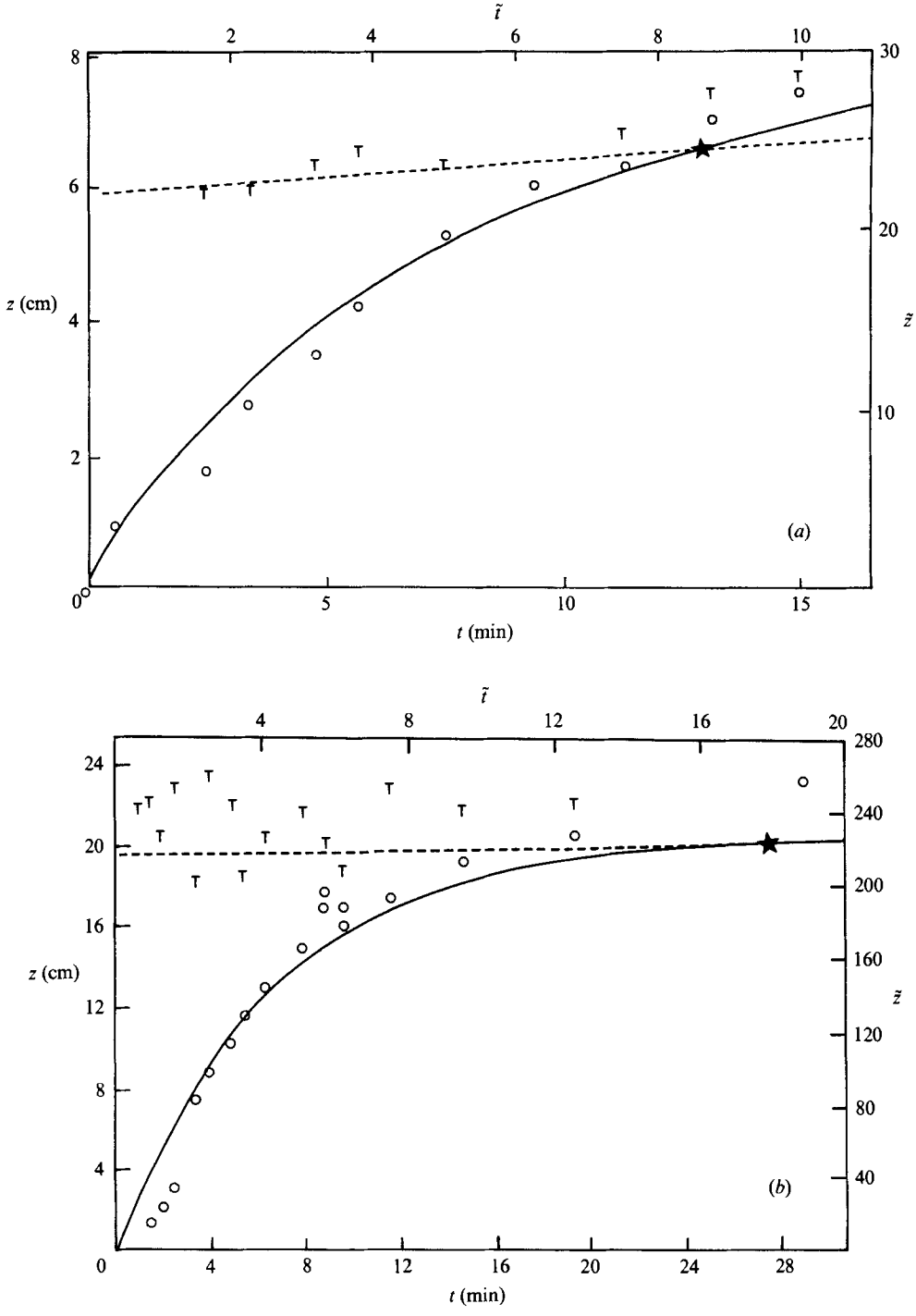

FIGURE 8. The elevations above a vertical source of a front (○) and the top of the fountain which is producing it (T), as functions of time. Both dimensional and dimensionless scales are shown. (*a*) First front of experiment A17. (*b*) First front of experiment A9. The source parameters of these experiments are listed in the captions to figures 4 and 2 respectively. The full line is equation (15) with $B = 0.25$; the dashed line is the linear approximation for z_m in each case, and ★ denotes the cross-over point.

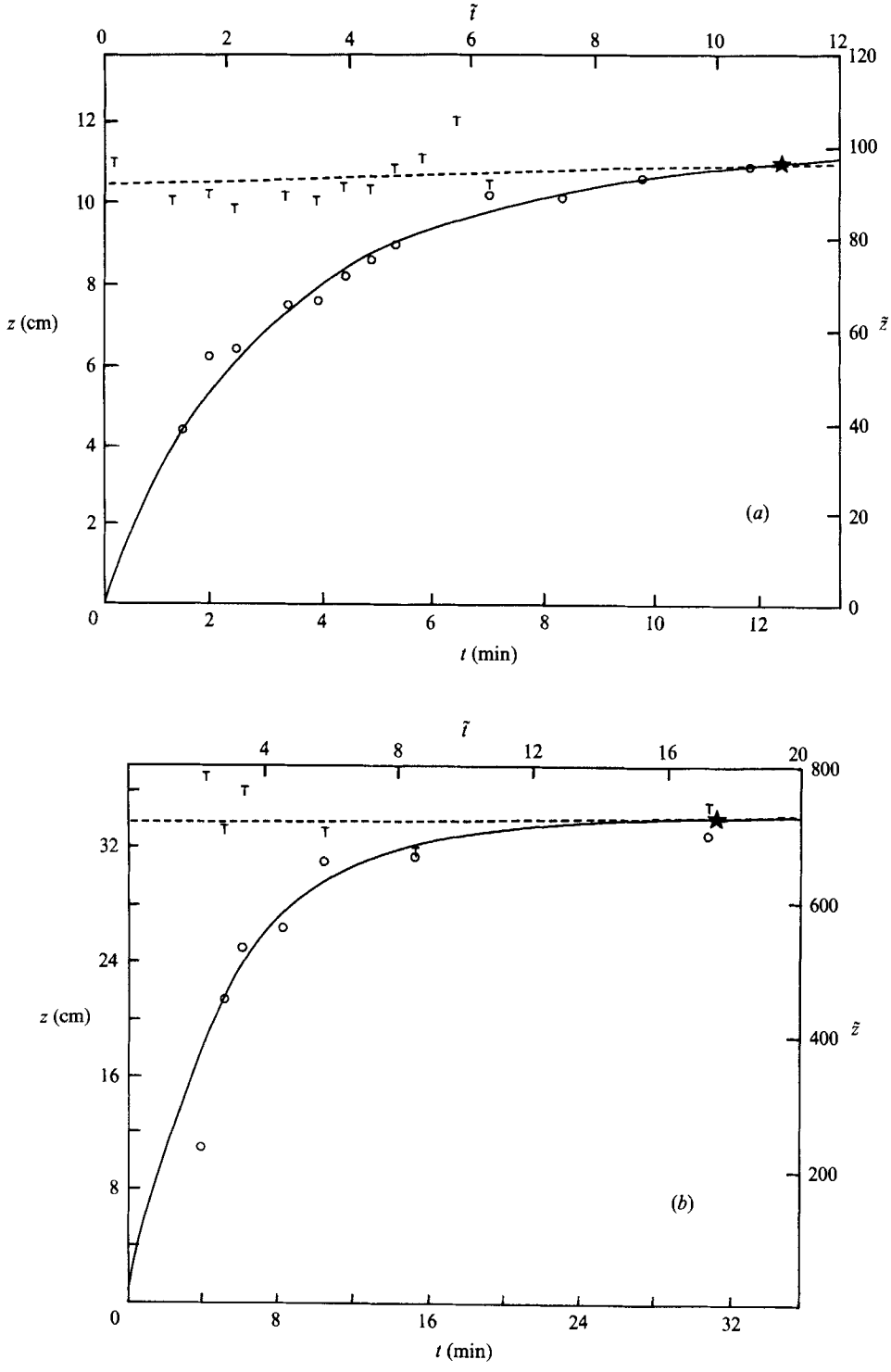

FIGURE 9. For caption see facing page.

experiments. The value of $\tilde{z}_{mi}$ was specified by (3) and z_s was the height of the source above the bottom of the tank. The value of B was adjusted to give the best fit of (15) to the measurements. Figures 8(*a*) and 8(*b*) present the plots for two cases of the vertical fountain and figures 9(*a*) and 9(*b*) present those for the 7° inclination. In all, nine experiments were carried out with a vertical source and five with a source inclined at 7° to the vertical, and usually two or three fronts were followed in each case. Mean values of B were $B = 0.25 \pm 0.03$ for the vertical and $B = 0.35 \pm 0.03$ for the inclined fountains, and there was no systematic variation with other parameters such as Fr_i. (A full listing of the results can be made available to interested readers.) No difference could be discerned for later fronts compared to the first front launched at $\tilde{t} = 0$, provided that, in each case, the value of $\tilde{z}_m$ used corresponded to the height of the fountain at the time the new front passed the level of the source. This means that the front rise is not strongly affected by the density profile below $\tilde{z}_m$. The first front has a uniform density above it and all later fronts move through a continuously stratified layer. It should be noted, however, that the accuracy of determining B by this fit is about $\pm 5\%$.

A value of $B = 0.35$ for the inclined fountain where the up- and downflows are separated is close to the entrainment to be expected for a pair of pure jets. The entrainment flux into a jet described by Gaussian profiles is

$$q_e = 2\pi\alpha \sqrt{2}\, U_0 r_0 \tag{17}$$

where α is the entrainment constant. The experiments of Albertson *et al.* (1950) are fitted by $\alpha = 0.057$ which gives $B = 0.161$. A pair of jets flowing in opposite directions would give $B = 0.322$ or about 10% less than the value obtained for the inclined fountain.

Note that once a generally applicable value of B has been found experimentally for a particular angle of inclination, the whole of the fountain behaviour and the character of the filling-box solution are determined by the initial Froude number Fr_i. In principle, we could calculate a one-parameter family of solutions for idealized starting conditions (e.g. $\tilde{z}_s = 0$), but we have chosen instead to give just a few illustrative examples of the procedure.

3.3.2. *The fountain height at later times*

Once the layer depth overtakes the fountain height, $\bar{\Delta}$ approaches more and more closely to Δ_0 and we can no longer rely on the linearized equation (10) and its consequence (13) as a basis for calculating the fountain height. At this stage we must also allow for the fact that buoyancy is being advected upwards above the top of the fountain.

The form of the density profile will be calculated as a function of time in the following section, but an important simplification can be made already on the basis of past and present experimental results. It has been shown by Campbell & Turner (1989) that the density profile, at the stage where the first front has passed the top

---

FIGURE 9. The elevations above a source inclined at 7° from the vertical of a front ○ and the top of the fountain T, as functions of time. Both dimensional and dimensionless scales are shown. (*a*) First front of experiment A8 ($r_0 = 0.187$ cm, $Q_0 = 13.8$ cm^3 s^{-1}, $\Delta_0 = 84.4$ cm s^{-2}, $Fr_i = 31.9$). The full line is equation (15) with $B = 0.35$. (*b*) First front of experiment A12 ($r_0 = 0.046$ cm, $Q_0 = 2.08$ cm^3 s^{-1}, $\Delta_0 = 42.2$ cm s^{-2}, $Fr_i = 250$). The full line is again equation (15) with $B = 0.35$. The dashed line on each figure is the linear approximation for z_m, and ★ denotes the cross-over point.

of the fountain and the volume of input fluid is comparable with or greater than the entrained fluid, can be well represented by a constant $\bar{\Delta}$ up to z_m where there is an abrupt change of gradient and a rapid decrease to the environmental value at z, the position of the front. The nearly constant density in the layer below z_m becomes an increasingly good approximation at larger times.

Using this assumption we can say therefore that the buoyancy added per unit time, namely $\Delta_0 Q_0$, is feeding a layer of depth z_m, area A and uniform buoyancy $\bar{\Delta}$. This layer is increasing in depth and has a flux of buoyancy out of its top because of the relative motion between the front and z_m. The buoyancy in the layer is $\bar{\Delta}Az_m$. The relative velocity through the top is $(Q_0/A - \mathrm{d}z_m/\mathrm{d}t)$ and the flux is $\bar{\Delta}A$ times this velocity. Equating the rate of inflow to the rate of change of buoyancy in the layer plus the loss across the top we obtain

$$\Delta_0 Q_0 = \left(Q_0/A - \frac{\mathrm{d}z_m}{\mathrm{d}t}\right)\bar{\Delta}A + \frac{\mathrm{d}(\bar{\Delta}Az_m)}{\mathrm{d}t}$$

$$= Q_0\bar{\Delta} + Az_m\frac{\mathrm{d}\bar{\Delta}}{\mathrm{d}t}, \tag{18}$$

or in dimensionless form

$$\frac{\mathrm{d}\bar{\Delta}}{\mathrm{d}\tilde{t}} = \frac{(\Delta_0 - \bar{\Delta})}{\tilde{z}_m}. \tag{19}$$

The exact form of (10) can be written as

$$\tilde{z}_m = \left(\frac{\Delta_0}{\Delta_0 - \bar{\Delta}}\right)^{\frac{1}{2}}$$

so that

$$\Delta_0 - \bar{\Delta} = \Delta_0/\tilde{z}_m^2 \tag{20}$$

and

$$\frac{\mathrm{d}\bar{\Delta}}{\mathrm{d}\tilde{t}} = \frac{2\Delta_0}{\tilde{z}_m^3}\frac{\mathrm{d}\tilde{z}_m}{\mathrm{d}\tilde{t}}. \tag{21}$$

Substituting (20) and(21) in (19) gives finally

$$\frac{\mathrm{d}\tilde{z}_m}{\mathrm{d}\tilde{t}} = \frac{1}{2}. \tag{22}$$

Thus we have arrived at the striking result that the top of the fountain should rise at just half the upward velocity of the first front. This is valid for large times under rather weak assumptions which are compatible with the observations. The same result holds in the early stages of rise for fountains produced by outflows close to the floor, for which z_s can be neglected when compared with z_m in (13). The result (22) is confirmed by our experimental observations, and by long runs of the numerical simulation.

The dimensionless rate of rise could increase above $\frac{1}{2}$ at intermediate times when the density at the fountain top is somewhat less than the mean density in the layer. The effect of decreasing the buoyancy flux out of the top of the layer is to decrease the density difference between the fountain and its environment and hence increase the rate of rise of the fountain.

3.4. *Theory for density distribution in the environment*

Since the molecular transport of density is negligible compared with the transport by convection, the fronts seen in the experiment define lines of constant density. Thus the density injected in the environment at the bottom moves upward with steadily reducing velocity until it reaches z_m. It enters the quasi-static layer between z_m and the free surface and subsequently moves upward with velocity Q_0/A. Relative to the free surface the density profile in this upper layer is constant. Although the density distribution as a function of time can be described by the Eulerian equation

$$\frac{\partial \Delta}{\partial t} + w\frac{\partial \Delta}{\partial z} = 0, \tag{23}$$

where w is the vertical velocity in the environment, it can be expressed in a simpler form by the Lagrangian relation

$$\Delta(z_e, t) = \Delta(z, t+t'), \tag{24}$$

where z_e is the elevation at which fluid effectively enters the new environment of the fountain (see figure 1), and t' is the passage time from z_e to z for a front starting at t, i.e. $t' = t'(t)$.

Equation (24) does not lead to an explicit form for the density distribution but the equations do give an implicit solution. In the particular case of the first front Δ_e, the value of Δ corresponding to z_e can be defined explicitly for $0 < t < t^*$ and so this value and (15) define the density profile, with (24) providing the time relation. For $t > t^*$ a numerical procedure can be used to predict the later location of a known value of Δ_e. The one adopted here uses integer values of the time increment δt for both t and t'. The buoyancy Δ_e is calculated using relations developed below for a series of integer multiples of δt. Then the time of entry of this front to the quasi-steady layer is calculated, using (16) to calculate t^* and converting this to an integer. This procedure defines the density at the elevation y below the free surface, which is given by the relative motion of the top of the fountain

$$\frac{dy}{dt} = \frac{Q_0}{A} - \frac{dz_m}{dt}. \tag{25}$$

Using the linear approximation (13) we obtain the dimensionless form

$$\frac{d\tilde{y}}{d\tilde{t}} = 1 - \tfrac{1}{2}\tilde{z}_r. \tag{26}$$

3.4.1. *Determination of density at entry to the environment*

Conservation of buoyancy flux in the fountain and the fluid it entrains gives the relation

$$\Delta_m(Q_e + Q_0) = \Delta_0 Q_0 + \bar{\Delta}(z_m + z_s)\, q_e, \tag{27}$$

where Δ_m = buoyancy of the fluid as it reaches the bottom of the tank, and the other quantities have been defined in §3.2. This defines the flow into the turbulent mixed layer which is formed from the fountain as it first spreads out along the bottom of the tank. The properties of this layer of thickness z_e and buoyancy Δ_e say have not been studied in detail but it was noted that the thickness and intensity of turbulence increase with Fr for a given tank size. If the time required to produce a well-mixed

bottom layer is small compared with the time required for a front to travel to z_m then the equation for conservation of buoyancy in the mixed layer is

$$z_e A \frac{d\Delta_e}{dt} = (\Delta_m - \Delta_e)(Q_e + Q_0). \tag{28}$$

An additional relationship linking $\bar{\Delta}$ to the other buoyancies is needed to give a closed set of equations. This is the conservation of buoyancy in the stratified layer between the bottom and z_m:

$$Q_0 \Delta_0 = A \frac{d}{dt}(\bar{\Delta}(z_m + z_s)) + Q_0 \Delta_T - A\Delta_T \frac{dz_m}{dt}, \tag{29}$$

where Δ_T is the buoyancy at $z = z_m$, the top of the fountain, and the last two terms allow for the loss of buoyancy due to the relative motion of the front and z_m (cf. (18)).

A solution for these equations is easily obtained for the first front condition. At $t = 0$ and until $t = t^*$, $\Delta_T = 0$ so (29) can be combined with (27) and (28) to give

$$\frac{d\tilde{\Delta}_e}{d\tilde{t}} + \frac{\tilde{Q}_e + 1}{\tilde{z}_e}\tilde{\Delta}_e = \frac{1}{\tilde{z}_e}(1 + \tilde{q}_e \tilde{t}), \tag{30}$$

where $\tilde{\Delta}_e = \Delta_e/\Delta_0$, i.e. the density difference is scaled with the density difference between the input fluid and the environment. The solution of this equation,

$$\tilde{\Delta}_e = \frac{1}{\tilde{Q}_e + 1}\left\{\tilde{q}_e \tilde{t} + \left(1 - \frac{\tilde{q}_e \tilde{z}_e}{1 + \tilde{Q}_e}\right)\left(1 - \exp\left(-\frac{\tilde{Q}_e + 1}{\tilde{z}_e}\right)\tilde{t}\right)\right\}, \tag{31}$$

is the sum of a linear term and a decaying exponential. The argument of the exponent $(\tilde{Q}_e + 1)/\tilde{z}_e$ increases in magnitude with increasing Fr because z_e was observed to change little in those experiments: it was between 2 and 4 cm in all cases. For the smallest Fr (about 9) the argument was about 0.6 so the exponential term was negligible for $\tilde{t} > 5$ or about one half t^*. For a large Fr of 100 the argument is about 6 and so the term is negligible for $\tilde{t} > 0.5$ or about one-fortieth of t^*. These values show that the mixed layer does not produce a jump in the density profile, nor does it have a large effect on the shape of the rest of the profile. This is also shown in the calculations of the profile discussed below.

3.4.2. *Calculation of the density profile*

The profile for time $t < t^*$ was calculated using (31) for the density at a time t_1 and (15) for the elevation at a time t_2 later. The profile for $t = t_1 + t_2$ was then plotted from the individual calculations. The three dashed profiles at the left of figure 5 are the results for the times corresponding to the measured points. These curves were computed using a mixed-layer thickness of 2.9 cm, a value chosen for numerical stability. The agreement is good for the higher elevations but the lower part of the calculated profile of course has a constant density. For the smallest time the profile was also calculated assuming no mixed layer. The result is shown as a dotted curve where it deviates from the previous curve; it agrees at the lower levels with the measurements but displays a jump at the top of the profile. These two calculations show that a uniform density distribution in the mixed layer is not an accurate description for small times after the start of the flow.

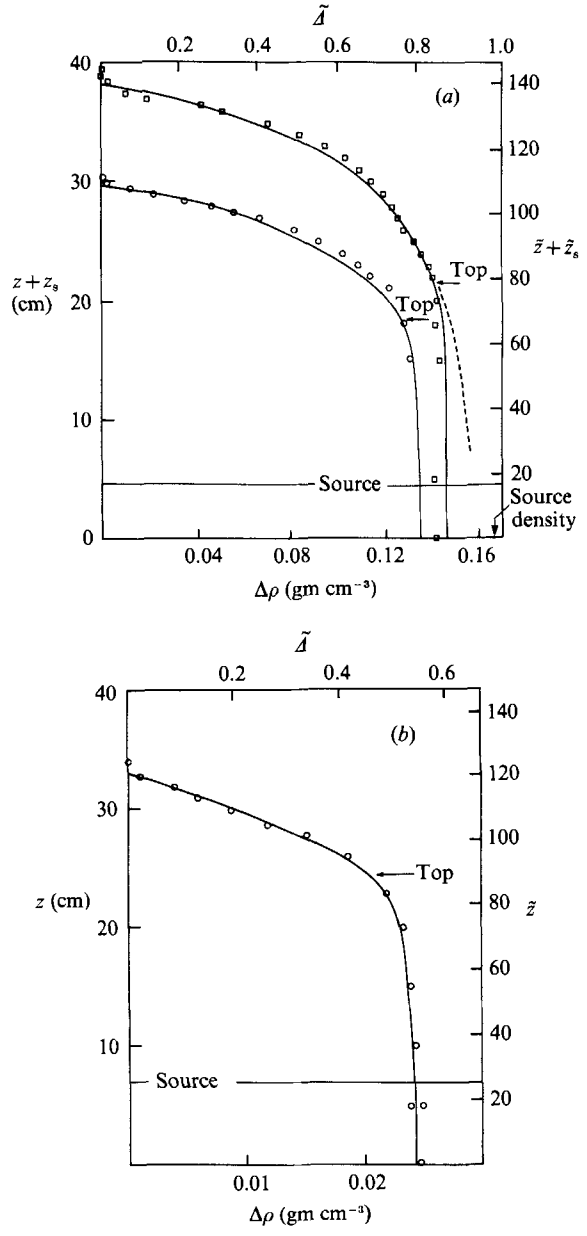

FIGURE 10. Density profiles produced by a vertical axisymmetric fountain. The full lines drawn represent the numerical simulation and the points are measured values. The dashed line of (*a*) is the limit as t tends to infinity. (*a*) Experiment A17 (source parameters as for figure 4): ○, time 2 h 0 min, $\tilde{t} = 73.8$; □, time 2 h 50 min, $\tilde{t} = 104.6$. (*b*) Experiment A14 ($r_0 = 0.271$ cm, $Q_0 = 13.7$ cm^3 s^{-1}, $\Delta_0 = 7.5$ cm s^{-2}, $Fr_1 = 17.7$). ○, time 1 h 30 min, $\tilde{t} = 56.9$.

The relationships defining the density profile at longer times are the combination of (27) and (28), together with (29). In dimensionless variables (dropping the ~ in the following three equations and the associated discussion) these are

$$\frac{d\Delta_e}{dt} = \frac{\bar{\Delta} Q_e + 1}{z_e} - \frac{\Delta_e (Q_e + 1)}{z_e} \tag{32}$$

and
$$\frac{\mathrm{d}\bar{\Delta}}{\mathrm{d}t} = \frac{z_r}{z_m}(1 - \Delta_T - \tfrac{1}{2}(\bar{\Delta} - \Delta_T)\, z_r), \tag{33}$$

with the initial conditions that $\bar{\Delta}, \Delta_e$ and Δ_T are zero at time zero. These equations are the core of the numerical solution for the density profile which proceeds as follows. For each time step δt the increases in Δ_e and $\bar{\Delta}$ are evaluated using the values of all variables at the start of the step. At the same time z_m and t^* are calculated at the start of the step using (13) and (16). Three quantities Δ_e, z_m and t^* are recorded for a time delay of t^* which is converted to an integer multiple of δt. As the calculation proceeds,

$$\Delta_T(t + t^*) = \Delta_e(t) \tag{34}$$

is linked to the depth below the free surface which is calculated simultaneously from (26). The density profile at a time t_f is evaluated by recording Δ_T as a function of y for the region between the free surface and the top of the fountain and Δ as a function of z for the variable time delay given in (24). The distance below the top of the fountain, corresponding to this value of Δ, is found by subtracting z from the value of z_m that existed when Δ was Δ_e, i.e. when the front was formed.

This numerical simulation of the density profile is compared with the measured profile in three typical cases. Figure 5 shows the initial period of an experiment in the smaller tank (using the three profiles on the right, at the longer times) and figures 10(*a*) and 10(*b*) plot results obtained in a larger tank for a longer period, and in all cases the agreement is good. In particular the measured density at the bottom of the tank $\tilde{\Delta}_e$ was compared with the value calculated in the numerical simulation. The agreement varies from $\pm 2\%$ to $\pm 10\%$ which indicates that some of the experimental parameters may not be defined accurately enough; the calculation is sensitive to both the diameter of the source and the location of the virtual source, determined as described in §3.1.

4. Line fountains

In all previous studies of jets and plumes there has been a close similarity between the two-dimensional and axisymmetric configurations. With the expectation that this similarity should also exist for fountains some experiments were undertaken and the analysis was adapted to describe the line fountain. Some new unsteady features were observed in our experiments, however, and we are led to the conclusion that the two-dimensional case is not as straightforward as was at first supposed.

4.1. *Apparatus and technique*

A tank 1.2 m long, 0.1 m wide, 0.6 m deep was constructed of acrylic sheet and a line source 0.1 m long was installed across the centre perpendicular to the long dimension of the tank. The source was a line of 0.5 mm holes spaced 5 mm apart on a circular pipe 8 mm in diameter. From the study of Crapper (1977) it was expected that the circular jets from the 0.5 mm holes would coalesce to a two-dimensional jet about 3.5 cm above the pipe and that the virtual origin would be at the outlet. The momentum flux from the holes should be conserved as the two-dimensional flow develops. However, the momentum of the flow from these holes cannot be predicted with certainty, so the value of b_0 was actually determined from experiments using the box-filling technique analogous to that described in §3.1. The tank was filled with salt water and fresh water was injected through the line of holes; a front formed as the

weakly buoyant jet impinged on the free surface and spread laterally. A plot of the square root of the elevation of the front as a function of time showed a linear variation for distances greater than 5 cm above the source, which corresponds to the entrainment rate $\propto z^{\frac{1}{2}}$ to be expected for a line jet, as set out below. Thus the flow in the jet was two-dimensional for $z > 5$ cm. The slope and intercept of the line indicated that the virtual origin was indeed at the outlet of the holes and that $b_0 = 0.00164$ cm if the entrainment coefficient is $\alpha = 0.106$, as determined by Kotsovinos & List (1977). The entrainment coefficient defines the entrainment velocity

$$v_e = \alpha w, \tag{35}$$

where w is the centreline velocity in the jet. Using this definition in the conservation equations for volume and momentum fluxes and assuming a Gaussian profile for velocity we obtain

$$w = 2^{-\frac{3}{4}}(m_0/\alpha z)^{\frac{1}{2}}, \tag{36}$$

$$b = 4\pi^{-\frac{1}{2}}\alpha z, \tag{37}$$

$$q = 2^{\frac{5}{4}}(m_0 \alpha z)^{\frac{1}{2}}, \tag{38}$$

where b is the half width of the velocity profile, measured where the velocity has fallen to 1/e of its central value w, and $m_0 = q_0^2/2b_0$ is the momentum flux per unit length from the source.

During the course of these calibration experiments it was found that damping screens had to be installed along the endwalls of the tank to overcome the lateral momentum of the jets along the surface. Without the screens the jet was deflected downward by the walls and formed a turbulent mixed layer with a thickness approaching half the depth of the tank (cf. Baines & Turner 1969, §4.1). Effective damping screens were made of a 15 cm diameter roll of commercial fly wire jammed vertically into the 10 cm tank width. When the lateral jet flowed through the screen, reflected from the wall and returned, the resulting mixed layer was about half the width of the outflowing jet as it reached the free surface. These screens were also used in all the experiments with line fountains.

In the six experiments with line fountains the tank was initially filled with fresh water and salt water was injected from the source. At the start, the source supply line was filled with a suspension of mica flakes so the initial 10 s of the fountain development could be easily observed in a sheet of light in the centre of the tank. Photographic floodlights were shone through slits 1 cm wide on each end of the tank and these illuminated the fountain and the front that formed in the environment. The elevation of the front could be read with an accuracy of 1 mm from a scale suspended in the sheet of light.

4.2. *Observations of line fountains and fronts*

The appearance of a line fountain is rather different from that of the circular one. The symmetrical flow illustrated in figure 3 does not remain steady; figure 11 shows two photographs of a more typical case. The top is wider and the downflow narrower than in the circular fountain. There does not appear to be a large difference between the profile of the upflow and that observed in a line jet: both show a similar linear expansion. The downflow does, however, vary considerably as the fountain develops and this affects the maximum height and observed profile.

The shape of the fountain in the initial period when the flow starts is best described by referring to the series of sketches in figure 12. The time interval between sketches

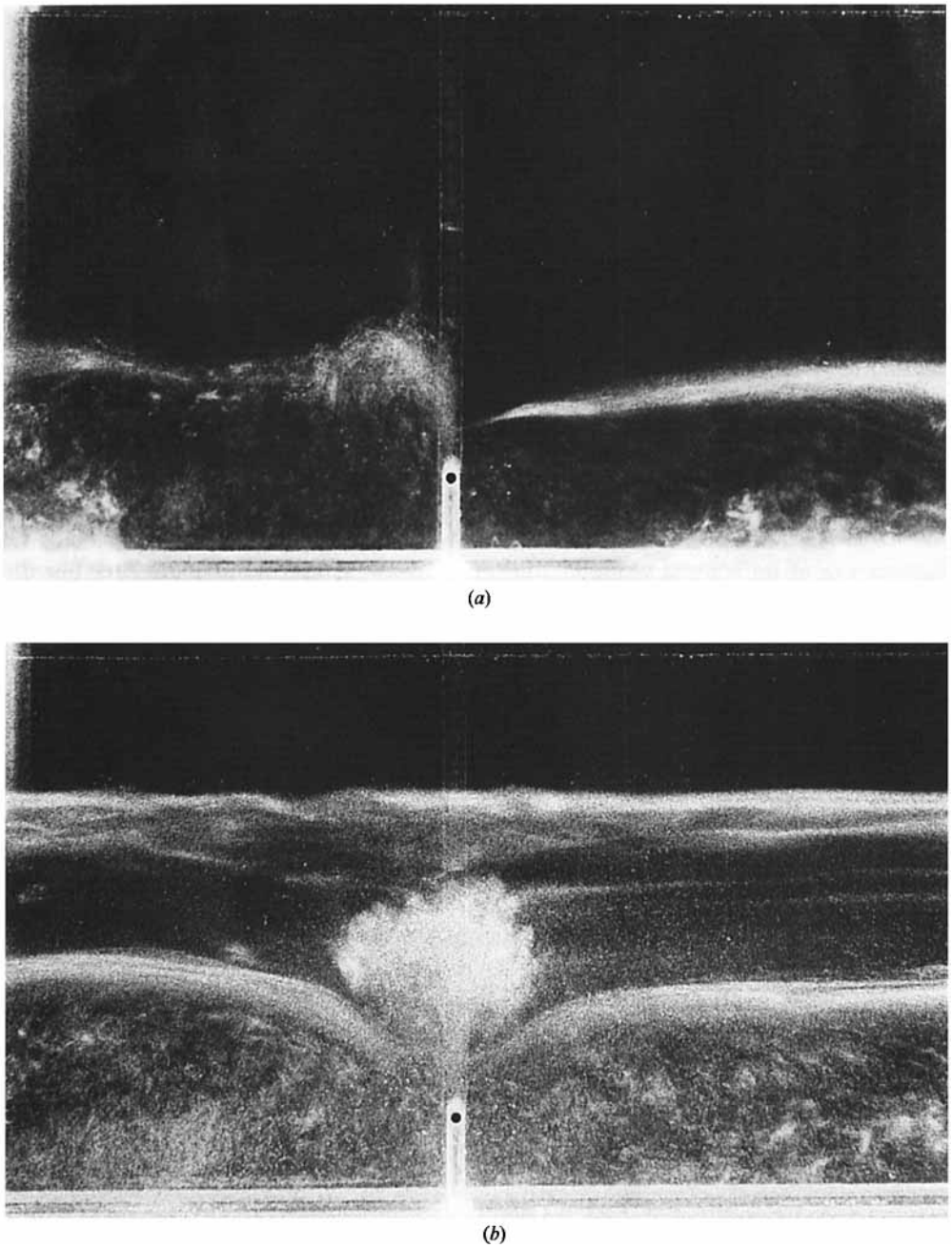

(a)

(b)

FIGURE 11. Photographs of a line fountain taken during experiment B6 ($b_0 = 0.00164$ cm, $q_0 = 0.464$ cm^2 s^{-1}, $\Delta_0 = 73.2$ cm s^{-2}). (*a*) 1 min after start of experiment, illustrating the non-symmetrical profile, with a single large eddy on the left which extends from the top to the elevation of the source. (*b*) 31 min after start, showing a symmetrical phase with large eddies at the top and a narrow downflow near the source. The first front has risen above the fountain and a second front (formed by the injection of dye at 30 min) lies below it and is distorted by the downflow.

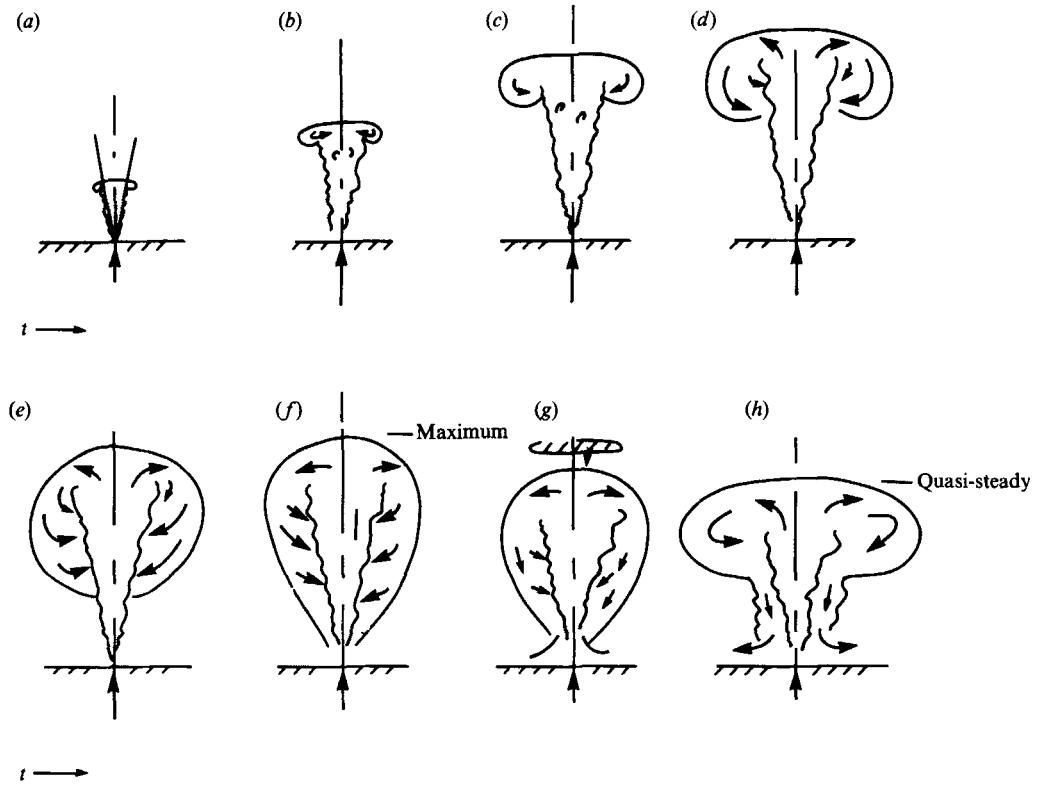

FIGURE 12. Sketches of the profile of a line fountain during the establishment of the flow. The time interval between sketches (in sequence from left to right, top to bottom) is about 10 s, $Fr \approx 8000$.

was about 10 s. Initially, the fountain is identical to a two-dimensional starting jet as shown in figure 12(*a*, *b*). The upflow is a linearly expanding turbulent flow which entrains surrounding fluid. Some fluid enters the head, which consists of two small volumes of rotating fluid. As time progresses the top advances more slowly and the head increases in width. Figure 12(*c*–*f*) shows this development. When the top reaches the initial maximum height the head is large and there is a downflow along the sides. Shortly thereafter the top drops in elevation and briefly leaves behind a layer of fluid. Since this is heavier than the environment it falls back into the fountain. The drop to the lower, quasi-steady height is probably due to the upflow now entraining heavier fluid from the downflow, so the buoyancy now has a larger negative value whereas the entrainment was previously from the environment. At this stage the head grows and becomes unstable. The top oscillates up and down and to each side, so a unique value of the elevation of the top is difficult to define.

The unsteadiness of the profile shape is more marked as the Froude number of the source increases. As the relative momentum of the upflow increases, there is an unsteady production of vorticity that is manifested in the oscillation sketched on figure 13. The photographs in figures 11(*a*) and 11(*b*) show the extremes of the shapes observed. At the start of the irregular cycle the profile was symmetrical (figure 11*b*) and the top rose to a maximum near that for the initial stage when the fountain was turned on (figure 12). The downflow was then deflected to one side; the top descended

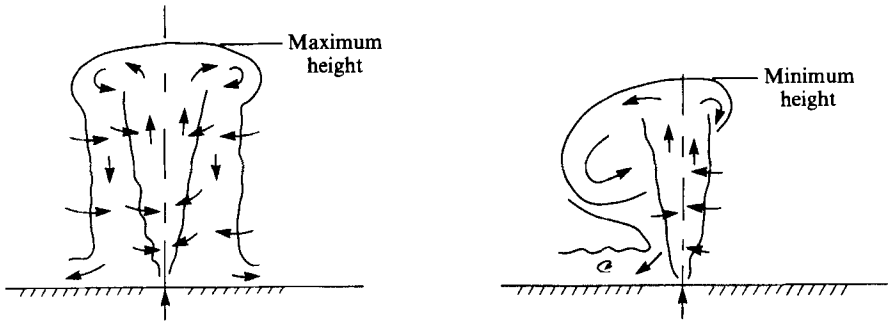

FIGURE 13. Sketches of the oscillation of a line fountain observed for a steady source flow at large Froude number. The transition between the two modes occurred at random intervals.

as the unsymmetrical lobe grew and reached a minimum height, as shown in figure 11(*a*). It oscillated irregularly between these extremes and heavy fluid was shed unevenly into the environment. On several occasions the large lobe was shed laterally and the rotation persisted until it reached the bottom of the tank. After the shedding the fountain increased in height to the maximum level.

Fronts in the environment were created at several times during the experiment by introducing fluorescein dye into the source. These progressed up to the top of the fountain and beyond (figure 11*b*). At all times after passing the top the fronts remained a constant distance below the free surface. The first front was easily identified in the density profiles measured at the end of the experiment.

4.3. *Analysis of the height of line fountains*

If it is assumed that the maximum height depends only on the momentum and buoyancy fluxes, as is the case for the circular fountain, then the dimensionless representation is

$$z_{\mathrm{m}} = \text{constant} \times m_0 f_0^{-\frac{2}{3}}, \tag{39}$$

where f_0 is the buoyancy flux per unit length. This can be written in terms of the Froude number as

$$\frac{z_{\mathrm{m}}}{b_0} = \text{constant} \times Fr^{\frac{4}{3}}, \tag{40}$$

where

$$Fr = \frac{w_0}{(b_0 \Delta_0)^{\frac{1}{2}}} = \sqrt{2}\left(\frac{m_0^3}{q_0^3 f_0}\right)^{\frac{1}{2}} \tag{41}$$

and b_0 is, as before, the half width of the source.

Figures 14(*a*) and 14(*b*) are plots of the observations made of the fountain heights. The measurements on figure 14(*a*) are those reported by Campbell & Turner (1989), though they were not plotted out in detail in that paper. The source was a slot ranging from 3 mm to 10 mm in width, so the Froude number was relatively small. The best-fit mean line gives the value of the constant in (40) as 0.65. The measurements made with the source described above are plotted in figure 14(*b*). The same line fits the data but the scatter is very much larger, and some of the variation can be explained in terms of the source geometry. For $Fr < 500$ (or $Fr^{\frac{4}{3}} < 4000$) the observed height is less than 5 cm which means that the jets from the source holes had

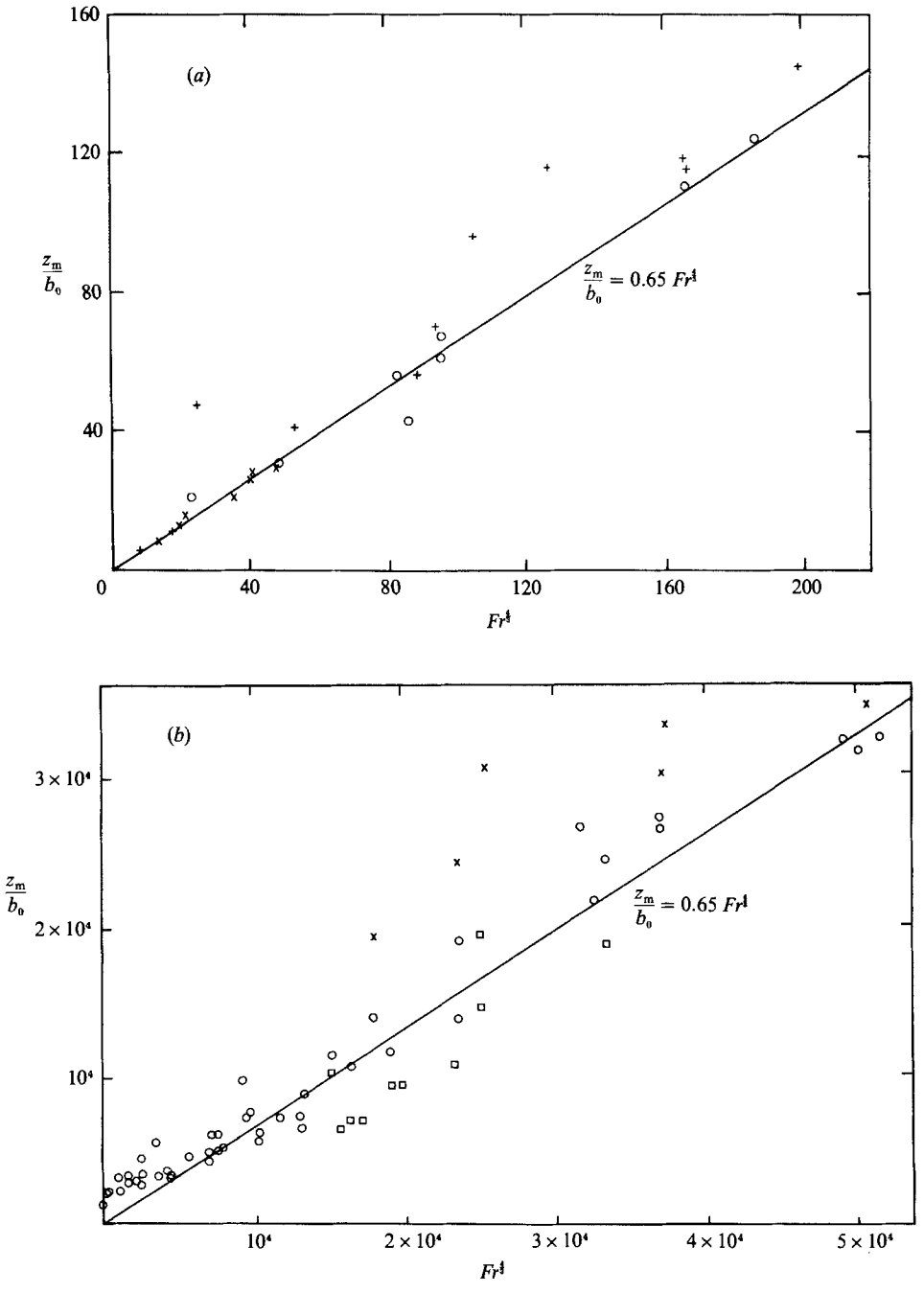

FIGURE 14. The height of line fountains as a function of the source Froude number. (*a*) Small-Fr measurements of Campbell & Turner (1989): +, $b_0 = 0.50$; ×, 0.325; and ○, 0.15. (*b*) Large-Fr measurements for the six experiments carried out using the tank and source described in the present paper. ×, initial maximum; ○, quasi-steady symmetrical height; and □, non-symmetrical experiments.

not coalesced to a line flow, so the maximum is that of circular fountains. In a few cases the fountain was clearly non-symmetrical and the height was about 20% lower than the mean line. A few observations were made of the initial maximum height as the flow was started and this was 30% above the mean line.

4.4. *Entrainment relations for a line fountain*

The form of the entrainment velocity as a function of elevation is developed by analogy with the axisymmetric fountain though, as will be seen below, the method is less satisfactory for the line fountain. First, dimensional consistency requires that

$$\frac{q_e}{q_0 Fr^{\frac{2}{3}}} = f\left(\frac{z}{b_0 Fr^{\frac{4}{3}}}\right), \tag{42}$$

where q_e is the volume flux entrained by the fountain between z_m and z. Second, the form of the function is assumed to be such that the same variation of v_e with z exists as for the simple two-dimensional jet. That is, from (35) and (36) we obtain

$$\frac{q_e}{q_0 Fr^{\frac{2}{3}}} = C - B\left(\frac{z}{b_0 Fr^{\frac{4}{3}}}\right)^{\frac{1}{2}}, \tag{43}$$

where B and C are constants. An attempt has been made to determine B from the motion of the fronts in the environment and the results are presented in §4.5. An approximate value for B can be obtained using the following comparison with a line jet. Differentiating (41), and allowing for the fact that q_0 includes entrainment into both sides of the line fountain, gives

$$v_e = \tfrac{1}{4} B q_0 b_0^{-\frac{1}{2}} z^{-\frac{1}{2}}. \tag{44}$$

For a jet, combining (35) and (36) leads to

$$v_e = \alpha^{\frac{1}{2}} 2^{-\frac{5}{4}} q_0 b_0^{-\frac{1}{2}} z^{-\frac{1}{2}}, \tag{45}$$

so that $$B = 2^{\frac{3}{4}} \alpha^{\frac{1}{2}} = 0.55, \text{ using } \alpha = 0.11.$$

4.5. *Elevation of a front*

The motion of a front is defined by the conservation of volume between the position of the front and the bottom of the tank. Thus the upward velocity of a front is

$$L \frac{\mathrm{d}z}{\mathrm{d}t} = q_0 + q_e, \tag{46}$$

where L is the length of the tank, and this is conveniently stated in dimensionless variables as

$$\frac{\mathrm{d}\tilde{z}}{\mathrm{d}\tilde{t}} = 1 + \tilde{q}_e, \tag{47}$$

where $$\tilde{z} = z/b_0, \quad \tilde{t} = tq_0/Lb_0, \quad \tilde{q}_e = q_e/q_0,$$

and time is measured from the commencement of flow. The Froude number Fr_0, Δ_0 and z_{mi} are defined as the values at this same instant. Substituting (43) in (46) leads to the dimensionless form

$$\frac{\mathrm{d}\tilde{z}}{\mathrm{d}t} = 1 + CFr^{\frac{2}{3}} - B\tilde{z}^{\frac{1}{2}}. \tag{48}$$

From (41), $Fr^{\frac{2}{3}}$ depends now on $\Delta_0^{-\frac{1}{3}}$ so that one can write linear approximations for Fr and z_m in the form

$$Fr^{\frac{2}{3}} = Fr_0^{\frac{2}{3}}(1+\tfrac{1}{3}\tilde{\Delta}), \tag{49}$$

$$z_m = z_{mi}(1+\tfrac{2}{3}\tilde{\Delta}), \tag{50}$$

where $\tilde{\Delta}$ denotes the mean density below the front $\bar{\Delta}$ made dimensionless with Δ_0 (cf. (10) and (13) and the notation in §3). In the time interval of the front rising to z_m all of the buoyancy excess which flows from the source is deposited in the layer of thickness $z_m + z_s$, where z_s is the height of the source, so that

$$\tilde{\Delta} \approx \tilde{t}\frac{1}{\tilde{z}_m+\tilde{z}_s} = \frac{\tilde{z}_r}{\tilde{z}_{mi}}\tilde{t}. \tag{51}$$

Equation (51) provides the final relationship needed to eliminate $\tilde{\Delta}$ and C from (48) and (49) and the resulting first-order differential equation defining the front is

$$\frac{d\tilde{z}}{d\tilde{t}} + B\tilde{z}^{\frac{1}{2}} = 1 + B\tilde{z}_{mi}^{\frac{1}{2}} + \frac{B}{3}\frac{\tilde{z}_r}{\tilde{z}_{mi}^{\frac{1}{2}}}\tilde{t}. \tag{52}$$

The only parameters in this equation are z_{mi} and z_r, which are defined by the initial conditions, and the entrainment function B. An analytical solution has not been found so (52) has been solved numerically using a fourth-order Runge–Kutta technique. The solution was repeated for three values of B, 0.5, 0.75 and 1.00 for each front produced in the six line fountain experiments. The results have been compared with the measured elevations and the agreement between the data and the numerical solution is also shown for two experiments, plotted in figures 15(*a*) and 15(*b*). The value of B for which the best fit was obtained for the several fronts of the six experiments was distributed fairly evenly between the above three values, and the accuracy of the measurements is not sufficient to permit a more accurate specification of B. The data show that there is a large variation of B that gives a reasonably good fit to the measurements, so that this is not a very sensitive method of determining this parameter. It is also probable that substantial variations of B can occur during an experiment, due to the oscillations in the fountain profile and consequently in the rate of rise of the front.

The mean value of B for line fountains is approximately 0.75, larger than the value of 0.55 obtained above for a line jet. Note, however, that in using (45) to obtain that estimate we made no allowance for the fact that the outer, downward-moving part of the fountain must influence the entrainment from the surroundings. If the downflow is treated as a line plume, then the argument used in §3.1 suggests that in this case too the downward velocity, and hence the entrainment velocity, will be independent of height. This does not match the $z^{\frac{1}{2}}$ dependence implied by (43), so that, in contrast to the axisymmetric case where the form of the entrainment is the same for the up- and downflows, it is not possible to retain the same functional dependence on z for both parts of the line fountain. Perhaps it is this fact which makes it so difficult to maintain a steady, vertical line fountain: it becomes unstable and falls over to one side when the upflow can no longer entrain fluid at a steady rate from the downflow, and changes to a state where direct mixing from the surroundings into the upflow is possible.

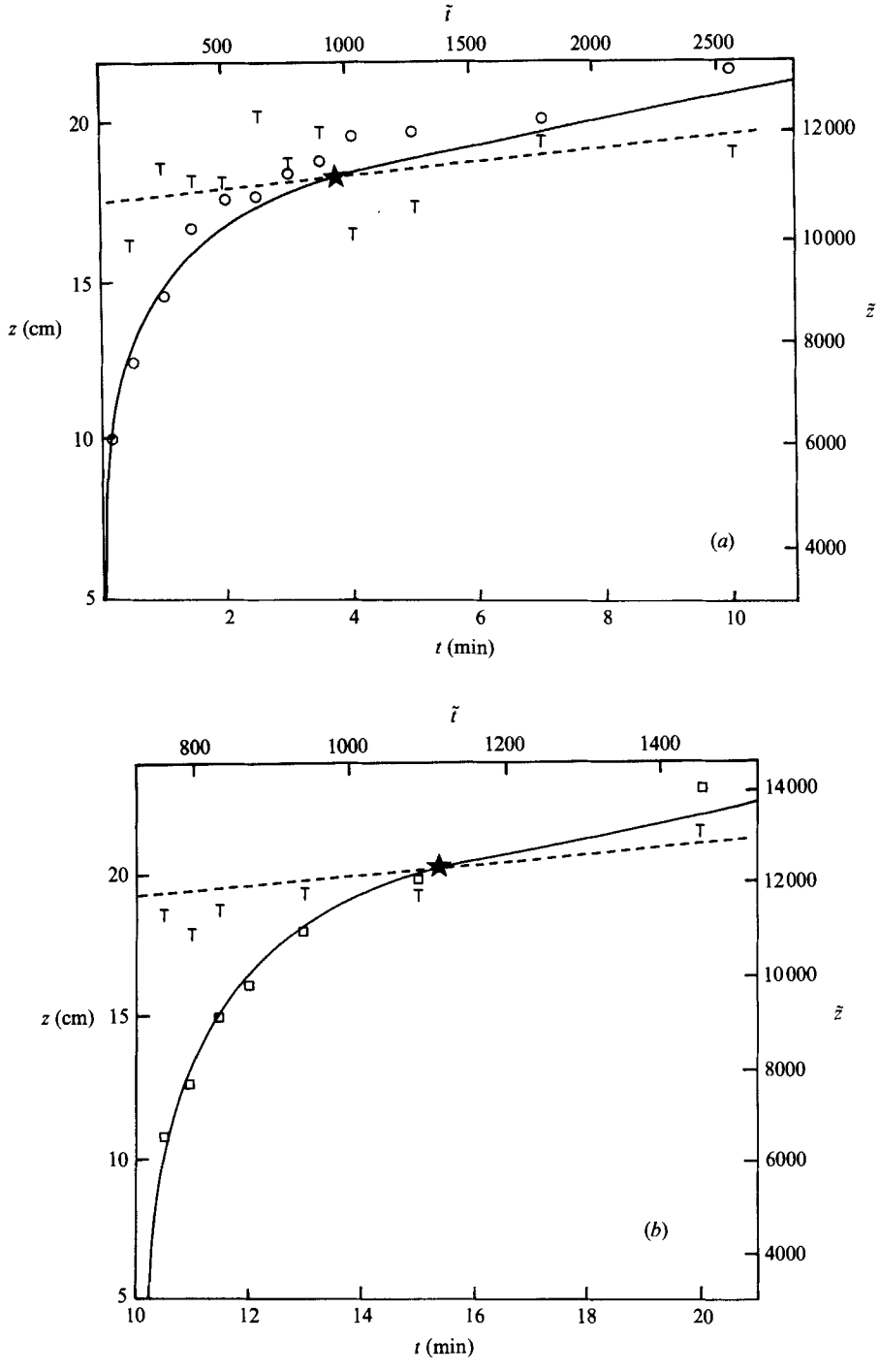

FIGURE 15. Position of fronts formed by a two-dimensional fountain, as a function of time. (*a*) First front of experiment B8. (*b*) Second front of experiment B8. (Source parameters listed in the caption to figure 16.) The full line is the solution of equation (52) with (*a*) $B = 1.0$ and (*b*) $B = 0.5$ and the dashed line is the linear approximation for z_m. The open circles and squares denote the measured front elevation, T the height of the top of the fountain and ★ the cross-over point.

4.6. *Density distribution in the environment*

A numerical simulation of the development of the density profile has been devised using the conservation equations, as was done for the axisymmetric case. However, the procedure is more complicated for line fountains because of the lack of an analytical expression for the position of a front. First, it can be assumed that in the region above the top of the fountain the density distribution is exactly that produced by the inflow into the fountain over the whole depth between the source and the fountain top; above this level it remains unchanged. The inflow between the level y measured from the (moving) free surface and the top of the fountain is given by

$$\frac{\mathrm{d}y}{\mathrm{d}t} = \frac{q_0}{L} - \frac{\mathrm{d}z_\mathrm{m}}{\mathrm{d}t}. \tag{53}$$

This leads, using (50) and (51), to the non-dimensional form

$$\frac{\mathrm{d}\tilde{y}}{\mathrm{d}\tilde{t}} = 1 - \tfrac{2}{3}\tilde{z}_\mathrm{r}. \tag{54}$$

The density of the fluid rising above the top of the fountain is equal to the density of a fluid parcel that left the mixed layer at a previous time determined by the above analysis of fronts (§4.5). The calculation of densities proceeds in time steps, using an analogous procedure to that set out in §3.4.2 for axisymmetric fountains. The conservation of buoyancy flux in the fountain gives (cf. (27))

$$\Delta_\mathrm{m}(q_0+q_\mathrm{e}) = \Delta_0 q_0 + c_1 q_\mathrm{e}\bar{\Delta}, \tag{55}$$

where most of the notation has already been defined, and c_1 is a coefficient of order unity which reflects the distribution of q_e and Δ over the height of the fountain.

The conservation of buoyancy Δ_e in the mixed layer leads to (cf. (28))

$$Lz_\mathrm{e}\frac{\mathrm{d}\Delta_\mathrm{e}}{\mathrm{d}t} = (\Delta_\mathrm{m}-\Delta_\mathrm{e})(q_\mathrm{e}+q_0), \tag{56}$$

where it is assumed that the buoyancy is uniform through the mixed layer and that the thickness z_e is constant. The third relation required is the conservation of buoyancy in the environment between the bottom of the tank and the top of the fountain (cf. (29))

$$(z_\mathrm{m}+z_\mathrm{s})\frac{\mathrm{d}\bar{\Delta}}{\mathrm{d}t} = \frac{q_0}{L} - \bar{\Delta}\frac{\mathrm{d}z_\mathrm{m}}{\mathrm{d}t} - \Delta_\mathrm{T}\left(\frac{q_0}{L} - \frac{\mathrm{d}z_\mathrm{m}}{\mathrm{d}t}\right), \tag{57}$$

where Δ_T is the buoyancy at $z = z_\mathrm{m}$.

At the start of a time step the density distribution is known, so that Δ_T, $\bar{\Delta}$ and c_1 can be determined. Equations (55), (56) and (57) are then used to calculate the change in Δ_e during the time step, and the value at the end of it. A linear variation of z_m is also assumed. Equation (52) is then integrated to predict the elevation where this value of buoyancy will be found at all subsequent times until t^*, the crossover time. The value of c_1 can be calculated by integrating the distributions of q_e obtained from (43) and Δ from the above procedure. However, this exact scheme has not been used in the simulations presented here. Instead we have used the approximation $c_1 = 1$, implying that the density distribution in the environment has little effect on the determination of the mean density. This is a reasonable simplification,

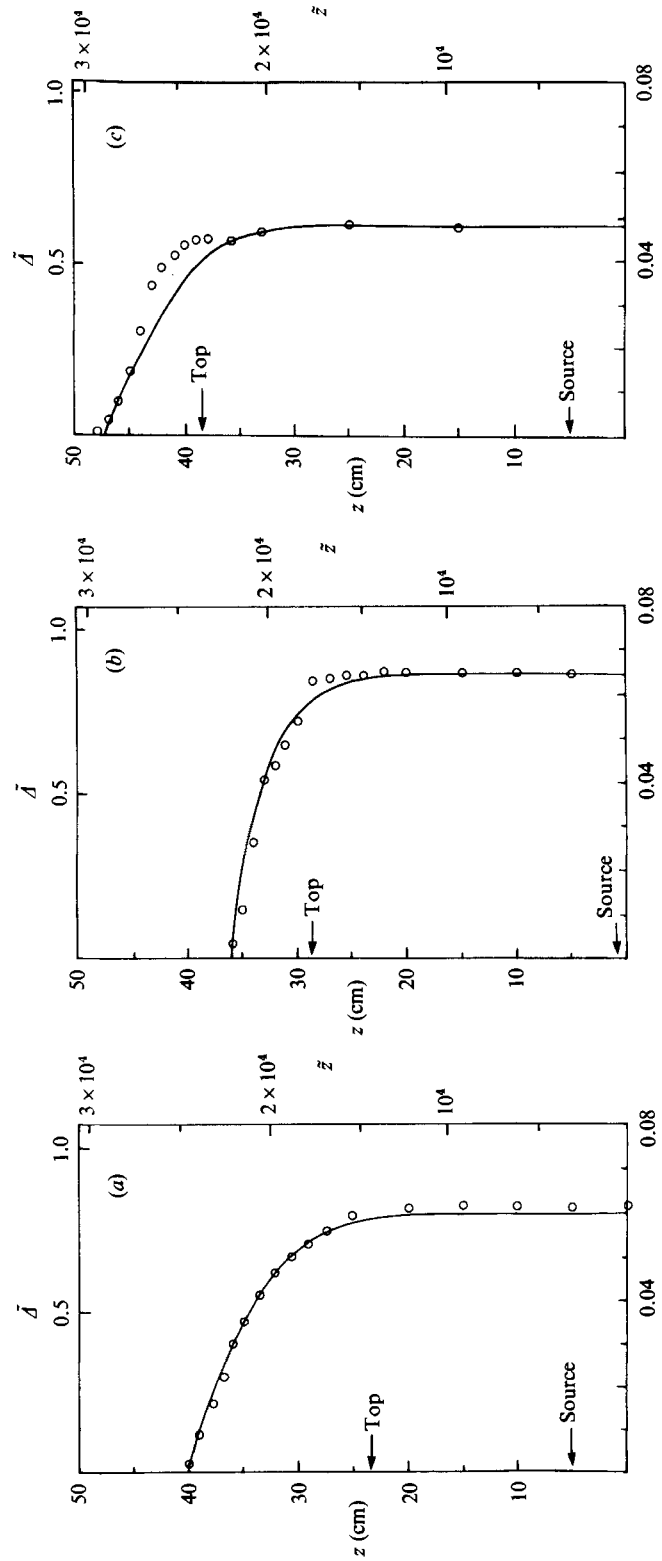

FIGURE 16. Density profiles produced by line fountains: the lines represent the numerical simulation, and the circles the measurements: (*a*) experiment B6 ($z_s = 5.0$ cm, $q_0 = 0.464$ cm^2 s^{-1}, $A_0 = 73.2$ cm s^{-2}); (*b*) experiment B7 ($z_s = 0.8$ cm, $q_0 = 0.464$ cm^2 s^{-1}, $A_0 = 73.2$ cm s^{-2}); (*c*) experiment B8 ($z_s = 5.0$ cm, $q_0 = 0.843$ cm^2 s^{-1}, $A_0 = 76.1$ cm s^{-2}).

particularly in view of the uncertainties in the value of $B = 0.75$ that has been used, and the fact that the oscillation of the height of the fountain has not been considered.

In carrying out the calculation two time intervals are defined. The first is the time from the start of the experiment to $t_f - t^*$, where t_f is the time where the distribution is to be determined. After Δ_e has been calculated, Δ_T is predicted for the time t^* later; (54) is integrated and the value of Δ_T is assigned to the coordinate y. In the second interval between $t_f - t^*$ and t_f the distribution between $z = 0$ and $z = z_m$ is determined by integrating to give Δ_e and then predicting z for a particular time using (52). This gives Δ as a function of z.

The density profiles for all six experiments on line fountains were calculated using this numerical simulation. Figure 16(*a–c*) presents the measured distributions as points and the simulations as the continuous lines for three of these experiments. The first two show the effect of changing the level of the source. Discharge and buoyancy flux were the same but the source elevation differed by 4.2 cm. The steeper density profile in figure 16(*a*) is the result of mixing over a larger volume below the source. The agreement between measurement and calculation is good in both cases but it should be noted that the calculated curves and points have been matched where the buoyancy is zero. This is necessary because the transient behaviour as the fountain and mixing layer are established is not included in the calculation. No unstable height oscillations were seen in experiment B6 but they were observed in the later stages of B7. Thus the deviation between the points and calculations in figure 16(*b*) near $z = 30$ cm is probably the result of the steepening of the density gradient produced by entrainment at higher levels than the nominal top of the fountain: entrainment always produces density gradient steepening. Figure 16(*c*) shows this effect very clearly. In experiment B8 the profile of the fountain oscillated over a large range throughout the experiment. The result is a density distribution that is steeper in that part of the layer between the free surface and the top of the fountain than is predicted by the numerical simulation assuming steady conditions.

The agreement between the measured and calculated buoyancies in the mixed layer was very good except in two cases where the conditions differed significantly from those assumed. When the Reynolds number of the jets from the source was small the fountain upflow remained laminar. Thus the fountain rose much higher than it would if it had been turbulent, and it entrained less of the turbulent downflow, so the measured buoyancy in the layer was higher than predicted.

5. Discussion and conclusions

We have presented measurements of the time evolution of the flow in fountains and the density distributions they produce in their environment over a wide range of input conditions. The excellent agreement between the experimental results and the theory developed to explain them indicates that our physical model gives a good description for the flow and mixing behaviour of both axisymmetric and line fountains. The results have been presented in dimensionless form, so that once the input parameters (the size and nature of the source vent, the rate of inflow and the density difference between the source fluid and its surroundings) are known the whole subsequent history can be calculated for fountains discharging into a region of constant cross-section. The only internally determined parameter, the rate of mixing into a fountain from its immediate surroundings (the constant B) has been evaluated from laboratory data, and the same numerical value can be applied to various prototype flows. Provided the fountains are turbulent the scale of the motion is

immaterial, and so is the working fluid (assuming of course the density differences are small and the fluids are miscible in any particular case), so that the same results can be applied to water, air or magmas. The case of a fountain surrounded by fluid with a very different viscosity has been considered by Campbell & Turner (1985). Other applications have been, or will be, treated in more detail elsewhere but in conclusion we return to the examples which motivated this study and make some general points about the meaning and use of our results in those and related contexts. We have not addressed the problem of fountains in a region with a varying cross-section, though this too should be amenable to numerical calculation once the geometry is specified (proceeding along the lines suggested for plumes in confined regions by Baines & Turner 1969).

The application to replenished magma chambers has recently been discussed by Campbell & Turner (1989), but there are several points made in that paper which can be clarified in the light of the present results. The need to consider the two stages of motion, before and after the first front overtakes the top of the fountain, is reinforced by the present study. It has been shown that the density gradient in the layer of hybrid magma below the top of the fountain continually decreases, and will become very small at large times. Using this result we have predicted theoretically that the fountain top will rise at close to half the speed corresponding to the rate of addition of fluid in the fountain. This provides a more satisfactory and quantitative explanation of the experimental results presented in the previous paper. With the line fountains we have observed a new phenomenon which might have some observable consequences for magma chambers. The spontaneous instability leading to the deflection of the fountain to one side could produce spatial non-uniformities, and extra variations in time even with a steady input. Our understanding of the line fountain and particularly of its unsteady behaviour is not as complete as it is for the axisymmetric case, and further experimental work is needed.

For the application to the heating of large buildings, in addition to providing the quantitative information on which detailed design criteria can be based, the results suggest overall strategies which might be adopted to make most efficient use of a given heat source. For example, starting with a completely unheated building the aim might be to produce a heated jet of air at the ceiling (drawn from outside, or from near the floor) which mixes initially with as much cold air as possible, by forming a fountain which turns back just above the floor. This flow should be continued, with the cold air allowed to flow out at the bottom, until the front of heated air has reached the floor (ideally at the same time as the bottom of the inverted fountain). At that time it would be more efficient to switch the intakes for the heating system to the inside of the building near the ceiling, so that no heated air is lost and the temperature gradually increases to the desired steady value at which it will be maintained.

It has also been shown that axisymmetric fountains inclined at a small angle to the vertical mix with their surroundings more rapidly than vertical fountains. A small deflection (7°) from the vertical increases mixing in two ways. First, the penetration is larger (by 17%) and second, the entrainment at all elevations is about 40% larger for the inclined fountain. This increase is of practical importance in engineering applications where intensive mixing is desirable, since it is obtained at no extra cost. It would be useful to study the variation with angle over a wider range to see if the entrainment can be further increased. In natural applications such as magma chambers, the angle of injection need not be exactly vertical, and so for that case too it would be relevant to explore this question further.

Another possible application of a fountain-like flow is to the destratification of water reservoirs. In summer, solar heating produces a layer of warm water on top of the deeper, colder water. This stable distribution isolates the colder water from the transfer of oxygen from the atmosphere and produces undesirable biological effects. There can also be a significant chemical stratification in some reservoirs. It is suggested that installing a ducted pump on the bottom of the reservoir with the outlet directed upwards (perhaps at a small angle to the vertical) would mix the layers by creating a fountain at the interface. From the results described in this paper it is evident that after a transient period there would be three layers. In between the original layers there would be a mixed region with its upper boundary at the top of the fountain and density which approaches that of the upper layer. Entrainment from the lower layer would contribute to the expansion of this middle layer, and the evolution could be calculated using the above analysis, modified to include the shrinking of the lower layer. One could also treat the flow and mixing produced by a pump installed at the surface and directed downwards, which may be a more efficient geometry if, as is usually the case, the upper layer is the thinner one.

The ideas described in this paper are currently being extended to include a distributed inflow or outflow of fluid at the level of the fountain source. A detailed theory and corresponding experiments are described by Baines & Reedman (1990), with the application to problems of building ventilation particularly in mind.

Most of the experiments described in this paper were carried out while W. D. B. was a Visiting Fellow at The Australian National University, where his work was supported by an International Cooperative Research Grant from the Natural Sciences and Engineering Research Council of Canada and also by NSERC Grant A-1066. We acknowledge Tony Beasley and Derek Corrigan for their technical help in preparing and carrying out the experiments, Ross Wylde-Browne for assistance with the photography, Karen Buckley for her patient wordprocessing of the many drafts of the manuscript and Clemantine Krayshek for drawing the diagrams. Myriam Bormans, Herbert Huppert and Paul Linden made valuable comments on an earlier draft.

REFERENCES

Albertson, M. L., Dai, Y.-B., Jensen, R. A. & Rouse, H. 1950 Diffusion of submerged jets. *Trans. ASCE* **115**, 639–697.

Baines, W. D. 1975 Entrainment by a plume or jet at a density interface. *J. Fluid Mech.* **68**, 309–320.

Baines, W. D. 1983 A technique for the direct measurement of volume flux in a plume. *J. Fluid Mech.* **132**, 247–256.

Baines, W. D. & Murphy, T. M. 1986 The temperature distribution in an enclosure produced by a forced plume. In *Proc. 8th Intl Heat Transfer Conf.*, pp. 1507–1512. Hemisphere.

Baines, W. D. & Reedman, T. J. 1990 The negative buoyant jet in a closed container. *J. Hyd. Engng, ASCE* (submitted).

Baines, W. D. & Turner, J. S. 1969 Turbulent buoyant convection from a source in a confined region. *J. Fluid Mech.* **37**, 51–80.

Batchelor, G. K. 1954 Heat convection and buoyancy effects in fluids. *Q. J. R. Met. Soc.* **80**, 339–358.

Campbell, I. H. & Turner, J. S. 1985 Turbulent mixing between fluids with different viscosities. *Nature* **313**, 39–42.

Campbell, I. H. & Turner, J. S. 1989 Fountains in magma chambers. *J. Petrol* **30**, 885–923.

CRAPPER, P. F. 1977 A note on the characteristics of a two-dimensional jet produced by a series of co-planar three-dimensional jets. *J. Indust. Aero.* **2**, 181–183.

GOLDMAN, D. & JALURIA, Y. 1986 Effect of opposing buoyancy on the flow in free and wall jets. *J. Fluid Mech.* **166**, 41–56.

KOTSOVINOS, N. E. & LIST, E. J. 1977 Plane turbulent buoyant jets. Part 1. Integral properties. *J. Fluid Mech.* **81**, 25–44.

KUMAGAI, M. 1984 Turbulent buoyant convection from a source in a confined two-layered region. *J. Fluid Mech.* **147**, 105–131.

MORTON, B. R. 1959 Forced plumes. *J. Fluid Mech.* **5**, 151–163.

MORTON, B. R., TAYLOR, G. I. & TURNER, J. S. 1956 Turbulent gravitational convection from maintained and instantaneous sources. *Proc. R. Soc. Lond.* A **234**, 1–23.

SEBAN, R. A., BEHNIA, M. M. & ABREAU, K. E. 1978 Temperatures in a heated jet discharged downward. *Intl J. Heat Mass Transfer* **21**, 1453–1458.

TURNER, J. S. 1966 Jets and plumes with negative or reversing buoyancy. *J. Fluid Mech.* **26**, 779–792.

TURNER, J. S. 1973 *Buoyancy Effects in Fluids.* Cambridge University Press, 367 pp.

TURNER, J. S. 1986 Turbulent entrainment: the development of the entrainment assumption, and its application to geophysical flows. *J. Fluid Mech.* **173**, 431–471.